THE M.I.T. BLOWDOWN COMPRESSOR FACILITY

by

Jack L. Kerrebrock

GTL Report No. 108 May 1972

GAS TURBINE LABORATORY
MASSACHUSETTS INSTITUTE OF TECHNOLOGY
CAMBRIDGE, MASSACHUSETTS

THE M.I.T. BLOWDOWN COMPRESSOR FACILITY

by

Jack L. Kerrebrock

GTL Report No. 108 May 1972

This research carried out in the Gas Turbine Laboratory, M.I.T., supported by the NASA Lewis Research Center under Grant NGL 22-009-383.

ABSTRACT

A Blowdown Compressor Test Facility has been developed which allows aerodynamic testing of full-scale compressor stages at low cost. The rotor is brought to speed in vacuum, a diaphragm is opened, and the test gas allowed to flow for a time of the order of one tenth second, during which the rotor is driven by its own inertia. Both "steady state" performance evaluation and detailed time resolution of the flow on the blade-passing time scale have been demonstrated in a preliminary way for a two-foot diameter transonic rotor with tangential Mach number of 1.2 and nominal pressure ratio of 1.6.

ACKNOWLEDGMENTS

This research was supported by the NASA Lewis Research Center under a program of cooperative research supervised by Dr. John C. Evvard, and funded by Grant No. NGL 22-009-383. It is the author's pleasure to acknowledge the contributions of Messrs D. N. Scogin and W. P. Patrick, who bore a large share of the responsibility for construction of the test facility. The Gas Turbine Laboratory staff, under the supervision of T. Christensen, also contributed greatly to this phase of the work, as did Mr. Alan Epstein. Prof. F. E. Marble made a major contribution in early discussions of the transient testing of turbomachines.

TABLE OF CONTENTS

NOMENCLATURE

A	flow area
a	speed of sound
c	blade chord
C_p	specific heat at constant pressure
D	diffusion factor, probe dimension
I	moment of inertia, intensity of light
i_c	incidence
L	length from scatterer
M	Mach number
p	pressure -- p(o), at t=0
R	particle radius
T	temperature or torque
t	time, blade thickness
U	flow velocity
V	volume
w	mass flow
α	air angle to chord line, dimensionless wave number
β	air angle to axis
γ	ratio of specific heats
γ^o	blade chord angle to axis
η_r	efficiency of rotor
λ	wave length
ϕ	camber angle

NOMENCLATURE (cont.)

σ	solidity
δ	fractional mass flow in boundary layer bypass
ω	angular velocity
ρ	density
Ω	inertia parameter -- Eq. (5)

Subscripts

1	supply tank
2	ahead of compressor
3	annulus behind compressor
4	dump tank
c	compressor
g	gas
r	rotor
T	radial station at tip
t	stagnation

LIST OF ILLUSTRATIONS

LIST OF ILLUSTRATIONS (cont'd)

LIST OF ILLUSTRATIONS (cont'd)

I. INTRODUCTION

Research and development on compressors has always been expensive and time consuming, in large part because proper simulation of both Mach number and Reynolds number has necessitated research on full sized full speed test rigs, with the attendant problems of mechanical stress and high power requirements. The expense of such testing has certainly precluded some fundamental study of compressor aerodynamics which is highly desirable. Test compressors operating in Freon have enabled high Mach number testing under less severe stress conditions, but power limitations and cost have limited the size and Reynolds number of these experiments. The size limitation, in addition to its effect on Reynolds number, causes the blade passing frequency in such test compressors to be quite high, thus limiting the possibilities for study of the unsteady flow on the time scale of blade passing.

The objective of the facility construction described here is to remove some of these restrictions on compressor testing, and make possible fundamental studies of compressor aerodynamics, both steady and unsteady, with full Mach number and Reynolds number simulation of practical compressors, and at modest cost. It is proposed that this be done by departing from the convention of operating the compressor in steady state. Since most aerodynamic phenomena of interest occur on time scales of the order of or much less than the rotational period of the compressor (which is larger than the flow time through even most multistage compressors), all relevant aerodynamic data can be acquired in a test lasting only a few rotational periods. This observation led to the conception of the blow-

down experiment, to be discussed here, in which a rotor is brought to speed in vacuum, then by bursting a diaphragm a test gas is passed through the rotor, from a supply tank to a dump tank. During the test time, the rotor is driven by its own inertia, eliminating the need for large powers.

This scheme has many advantages. A relatively small amount of test gas is used, so its properties can be chosen without too much regard for cost. Choice of a high molecular weight gas allows testing at high Mach numbers without serious stress problems. Elimination of the high powered drive allows large diameter tests at reasonable cost. The large size, in combination with low-sound-speed gases, lowers the blade passing frequency to a level resolvable by modern pressure transducers. The freedom of choice of test gas opens up possibilities for optical diagnostics which are not feasible in steady state experiments.

Of course the technique is not without its problems. Some of these will be discussed in the following pages. But the development has been carried to the point of preliminary testing of a large transonic rotor, thus demonstrating the basic feasibility of the testing technique. Parallel developments of the diagnostic techniques mentioned above have also progressed to the point of demonstration of feasibility, and will be described briefly here.

II. THE BLOWDOWN FACILITY

The blowdown compressor facility is shown schematically in Fig. (1). It consists of a supply tank, initially separated from the compressor by a diaphragm, the compressor test section, and a dump tank into which the compressor exhausts. It is envisioned that, after the diaphragm ruptures the gas will expand from the supply tank, which essentially behaves as a stagnation plenum, not as a chock tube driver. This requires that the test time be large compared to the acoustic period of the supply tank. As the supply gas expands, its pressure and temperature decrease, but the rotor slows because it is doing work, and as we shall see below, by proper matching, the rotors tangential Mach number can be made nearly constant throughout the test time. If the discharge orifice remains choked, this in turn implies that the axial Mach number is constant. The condition on the dump tank volume is then that the discharge orifice not unchoke during the desired test time. The initial dump tank pressure is determined by the power requirements for bringing the rotor to speed. As we shall see, the vacuum requirement is modest. The rotor torque can be determined with high precision by monitoring its deceleration.

In the following sections, the dynamics of the blowdown and rotor deceleration will be described, after which the criteria for sizing the facility will be given.

2.1 Gas Supply

Let V_1 be the volume of the supply tank, and suppose, as mentioned above, that it behaves as a uniform plenum. The density in it then decreases with time according to

$$\frac{d}{dt}(\rho v_1) = -\rho_2 u_2 A_2 \tag{2.1}$$

If we assume, subject to later verification, that the Mach number, M_2, at the compressor face is constant throughout the flow time, then

$$\rho_2 u_2 = A^*/A(M_2)(\rho u)^*_{①} = [A^*/A(M_2)]\left(\frac{2}{\gamma+1}\right)^{\frac{\gamma+1}{2(\gamma-1)}} \rho_1 a_1$$

if we assume that $M_1 << 1$ so that $\rho_1 a_1$ is equal to the stagnation value. (This is correct to within 0.3 percent for the present experiment.) The flow being isentropic, $a_1 \alpha \rho_1^{\frac{\gamma-1}{2}}$

so that Eq. (2.1) becomes,

$$\left[\frac{\rho_1}{\rho_1(0)}\right]^{-\frac{\gamma+1}{2}} \frac{d}{dt}\left[\frac{\rho_1}{\rho_1(0)}\right] = -\frac{a_1(0)A_2}{V_1}\frac{A^*}{A}(M_2)\left(\frac{2}{\gamma+1}\right)^{\frac{\gamma+1}{2(\gamma-1)}}$$

Integrating this leads to

$$\frac{\rho_1}{\rho_1(0)} = \left[1 + \frac{\gamma-1}{2}\left(\frac{2}{\gamma+1}\right)^{\frac{\gamma+1}{2(\gamma-1)}} \frac{a_1(0)A_2}{V_1}\frac{A^*}{A}(M_2)t\right]^{-\frac{2}{\gamma-1}} \tag{2.2}$$

The pressure and temperature are then given by the isentropic relations

$$\frac{p_1}{p_1(0)} = \left[\frac{\rho_1}{\rho_1(0)}\right]^{\gamma}, \quad \frac{T_1}{T_1(0)} = \left[\frac{\rho_1}{\rho_1(0)}\right]^{\gamma-1}$$

It is convenient to define a characteristic time, τ_g, for the supply tank as

$$\tau_g = \frac{V_1}{\frac{\gamma-1}{2}\left(\frac{2}{\gamma+1}\right)^{\frac{\gamma+1}{2(\gamma-1)}} a_1(0)\, A_2\, A^*/A(M_2)} \tag{2.3}$$

so that (2.2) takes the form $\rho_1/\rho_1(0) = (1 + t/\tau_g)^{-\frac{2}{\gamma-1}}$

2.2 Rotor Deceleration

Let the moment of inertia of the rotor, and all parts which rotate with it, such as the drive motor, be I, and its angular velocity ω. The deceleration

of the rotor is then given by

$$I \frac{d\omega}{dt} = T \tag{2.4}$$

where T is the torque acting on the rotor due to the gas flow. It is in turn related to the temperature rise across the rotor by $\omega T = \rho_3 u_3 A_3 C_p (T_{t_3} - T_{t_2})$. The compressor mass flow $\rho_3 u_3 A_3$ has been distinguished from the mass flow out of the supply tank, $\rho_2 u_2 A_2$, to allow for some flow by passing the compressor through boundary layer bleeds. To account for this, let $\rho_3 u_3 A_3 = \rho_2 u_2 A_2 (1 - \delta)$, then Eq.(2.4) becomes

$$\omega \frac{d\omega}{dt} = - \frac{\rho_2 u_2 A_2 C_p T_{t_1}}{I} (T_{t_3}/T_{t_2} - 1)(1 - \delta)$$

From Eq.(2.1), $\rho_2 u_2 A_2 = - d(\rho_1 V_1)/dt = \rho_1(0) V_1 \left[\frac{2}{\gamma-1} (1 + t/\tau_g)^{-\frac{\gamma+1}{\gamma-1}} \right] / \tau_g$

while $T_1 = T_1(0) [1 + t/\tau_g]^{-2}$, so that

$$\omega \frac{d\omega}{dt} = - \frac{2}{\gamma-1} \frac{\rho_1(0) V_1 C_p T_1(0)(1-\delta)}{I \tau_g} (1 + \frac{t}{\tau_g})^{-\frac{3\gamma-1}{\gamma-1}} \left(\frac{T_{t_3}}{T_{t_2}} - 1 \right)$$

Integrating, we find

$$(\frac{\omega}{\omega(0)})^2 = 1 - \frac{2(1-\delta) V_1 p_1(0) (T_{t_3}/T_{t_2} - 1)}{(\gamma-1) I \omega^2(0)} \left[1 - (1 + t/\tau_g)^{-\frac{2\gamma}{\gamma-1}} \right]$$

Defining $\Omega = \frac{2(1-\delta) V_1 p_1(0) (T_{t_3}/T_{t_2} - 1)}{(\gamma-1) I \omega^2(0)}$

$$f(t/\tau_g) = 1 - (1 + t/\tau_g)^{-\frac{2\gamma}{\gamma-1}} \tag{2.5}$$

We write this as

$$(\frac{\omega}{\omega(0)})^2 = 1 - \Omega f$$

The function $f(t/\tau_g)$ is shown in Fig. 2 for $\gamma = 1.4$.

If the rotor is to run at constant tangential Mach number during the test time, $[\omega/\omega(0)]^2$ should behave identically in time to the square of the speed of sound, or to $T_1/T_1(0)$, i.e. as $(1 + t/\tau_g)^{-2}$. This dependence is shown in Figure 2. Now by choosing Ω, we want to make $[\omega/\omega(0)]^2$ as close to $T_1/T_1(0)$ as possible. It is shown for two values of Ω in Figure 2, $\Omega = 0.40$, and 0.35. There is a rather good fit for $\Omega = 0.40$ out to $t/\tau_g \simeq 0.2$, the maximum deviation being about 2.5 percent in $[\omega/\omega(0)]^2$ or about 1.3 percent in $[\omega/\omega(0)]$.

Tailoring of the rotor to give the proper value of Ω implies adjusting its moment of inertia, other things being fixed, but note that for a given rotor, Ω can be adjusted by varying the initial pressure in the supply tank. It is important to note also that Ω depends on $(T_{t_3}/T_{t_2} - 1)/\omega^2(0)$. If the velocity triangles remain similar as the rotor speed is varied, the temperature rise is roughly proportional to $\omega^2(0)$, so the rotor if tailored to give the right Ω at design corrected speed, remains so at reduced corrected speed also.

2.3 Dump Tank

To estimate the size of the dump tank, assume an average density, $\bar{\rho}_4$ in it. Then

$$\frac{d}{dt}(\bar{\rho}_4 V_4) = \rho_2 u_2 A_2$$

$$= \rho_1(0) V_1 \frac{2}{\gamma-1} \frac{1}{\tau_g} (1 + \frac{t}{\tau_g})^{-\frac{\gamma+1}{\gamma-1}}$$

and integrating

$$\frac{\bar{\rho}_4 V_4}{\rho_1(0) V_1} = 1 - (1 + t/\tau_g)^{-\frac{2}{\gamma-1}} \qquad (2.7)$$

For $t/\tau_g = 0.2$, this gives $\bar{\rho}_4 V_4/\rho_1(0)V_1 = 0.60$. Assuming that $\bar{T}_4/T_1(0) \simeq 1$, $\rho_4 V_4/\rho_1(0)V_1 \simeq .60$ at $t/\tau_g = 0.2$. But at this point $\rho_1/\rho_1(0) = [T_1/T_1(0)]^{\gamma/\gamma-1}$ $\simeq .27$, so if the compressor exit orifice is to be choked (without accounting for the pressure ratio of the compressor), we must have $\rho_4/\rho_1(0) \simeq .14$, and this gives $V_4/V_1 \simeq .60/.14 \simeq 4$.

2.4 Time Scales and Sizing of Facility

A prime requirement placed on the sizing of the facility was that events on the blade-passing time scale be easily resolved by available instrumentation. Miniature strain-gage type pressure transducers, such as the Kulite brand,have resonant frequencies in the range of 10^5 Hz. Preliminary studies indicated that such transducers could be built into cavities, to yield stagnation and static pressures, the assembly having frequency response fairly flat to 2×10^4Hz. Such pressure probes will be discussed in Section IV. It was arbitrarily decided that measurement of the fourth harmonic of blade passing for a 23 bladed rotor would suffice. At a tip speed of 1000 ft s^{-1} this leads to a 2 ft diameter rotor, turning at 160 rps.

A test time of about 0.1s was selected, giving 16 revolutions of the rotor during the test. For $t/\tau_g = 0.2$, this requires $\tau_g \simeq 0.5$ s. An axial Mach number $M_2 = 0.5$ was selected as typical, and a hub/tip radius ratio of 0.5. From Equation(2.3) this leads to $V_1 \simeq 80$ ft^3. A 5 ft long by 5 ft diameter supply tank was selected, with a volume of 100 ft^3. The largest dump tank which could be fitted through the laboratory door was about 5 ft diameter by 15 ft long, giving 300 ft^3. This meets the choking requirement for a compressor pressure ratio of 1.2 at $t/\tau_g = 0.2$.

The resulting facility is shown to scale in Figure 3. In addition to the features already mentioned, the test section is equipped with an annular boundary layer bleed just upstream of the compressor, to remove flow disrupted by the diaphragm. It removes about 10 percent of the total flow. The rotor is cantilevered forward from a strut-mounted centerbody, so that the inlet flow is undisturbed. Details of the test section and instrumentation will be discussed in later sections.

2.5 The Diaphragm

The diaphragm for this facility must satisfy requirements quite unlike those met by shock tube diaphragms. It is large (two foot diameter) and supports a relatively small pressure difference of about 1/2 atmosphere. To minimize disruption of the flow, more than four petals were desired. Complete opening of the diaphragm in about 10 milliseconds was set as a goal, this being 10 percent of the nominal test time.

Because of the severity of these conditions, a program of diaphragm development was initiated early in the planning stage of the facility using a six inch diameter mockup of the compressor inlet. A large number of diaphragm materials and several bursting techniques were tried, with discouraging results. The one method which has proven fairly successful is to cut an aluminum diaphragm with high explosive strips. Figure 4 shows the method schematically. "Detasheet" (Dupont) .015 inch thick is backed by "double stick" plastic tape, then sliced into strips .055 inch wide, and stuck to the diaphragm in a star pattern as shown. A leader is attached to the center of the star, and carried through the test section wall to a small chamber, where it is initiated by a dynamite cap.

The explosive is applied to the low pressure (about 0.1 mm Hg) side of the diaphragm, facing the compressor. This is important for two reasons. It minimizes stirring of the supply gas by the explosion, and it also minimizes the chance of blowing diaphragm material into the test section.

A dead soft grade of aluminum (1100-0) .025 inches thick has proven most successful for operation at pressures near 500 mm Hg. Harder grades of aluminum tend to produce petals which spring back from the test section wall.

A sequence of frames from a high speed movie of the diaphragm opening is shown in Figure 5. The bright light outlining the petals is from the explosion. The film speed is 750 frames per second.

2.6 Gas Mixtures and Preparation

A detailed and comprehensive study of high molecular weight gas mixtures for wind tunnels was reported by Chapman.[1] Mixtures of heavy noble gases, in particular Argon, with heavy Freons offer the possibility of considerably lower speeds of sound than in air, with average ratio of specific heats maintained at 1.4. Some typical mixtures and their properties are presented in Table I, abstracted from Ref. (1). For the initial series of tests the Argon, 82%, Freon 12 18% mixture was selected for its low cost. It gives a room-temperature speed of sound of 820 ft s^{-1} or 0.716 of that of air. The cost, for one supply tank filling, is about $10.

The Argon-Freon mixture is prepared by boiling the liquid Freon 12 in a water heated exchanger, then mixing in a long filling line, the

TABLE I

Properties of Mixtures of
Polyatomic Gases with Argon

Polyatomic Gas	Mole Fraction	Mol. Wt. rel. to Air	Viscosity rel. to Air
SF_6	0.14	1.91	1.12
$CC\ell_2F_2$ (Freon12)	0.20	1.93	1.02
$CBrC\ell F_2$	0.19	2.18	1.03

mass flows of Argon and Freon being measured by rising-float flowmeters. This system is shown schematically in Fig. 6. It is capable of handling other Freon-Argon mixtures, and with slight modifications trace gases can be added uniformly for diagnostic purposes.

III. INSTRUMENTATION AND DATA ACQUISITION

Data from this experiment fall into several classes according to time scale:

1) essentially D.C. data, such as temperatures, initial pressure in the supply tank, etc. These are all read on conventional instruments and recorded manually.

2) data which varies on the blowdown time scale of about 0.1 sec, including supply tank and dump tank pressures, rotor inlet and outlet pressure (averaged over many blade passing periods), and rotor speed.

3) data which varies on the blade-passing time scale, including static and stagnation pressures ahead of and behind the rotor, flow velocity and static temperature.

All data of categories 2) and 3) are recorded on a 14 channel wide band FM tape recorder with frequency response from DC to 80 KHz at 120 inch per second tape speed. One channel is reserved for a time base generated from an oscillator (200 KHz) and another records the signal from a magnetic pickup adjacent to a 115 tooth gear mounted on the compressor shaft. In this way, the data can be recovered from the tape one channel at a time, referenced either to the absolute or the rotor time base. Comparison of the two time bases gives the deceleration of the rotor.

The data can be played back at reduced tape speed of $1\frac{7}{8}$ inches per second, for a 64 fold expansion of the time scale, either into a strip chart recorder, or oscilloscope, or into a two channel analog-to-digital converter arranged to interface with the M.I.T. Computation Center.

Characteristics of the principal items of instrumentation are given

In Table II. As the fast response static and stagnation pressure probes were developed for this experiment, they will be discussed further in the following section.

3.1 Fast-Response Pressure Probes

Two types of probes have been designed and evaluated, all based on the used of Kulite strain gage pressure transducers. They are (1) a stagnation pressure probe with low angular sensitivity, and (2) a static pressure probe.

Each of those probes must satisfy two requirements. The physical dimension of the probe must first be small enough, relative to the smallest flow feature to be resolved, so that the probe can give the desired resolution. Thus, if the blade spacing is S and the probe dimension D, the probe size limits the resolution to a fraction $\varepsilon = D/S$ of the blade spacing. Secondly, for this measurement to be useful the frequency response of the probe should be flat to a frequency $f > \omega r/\varepsilon S = (\omega/2\pi)(B/\varepsilon)$ which allows temporal resolution of phenomena of the scale εS in rotor coordinates (B is the number of blades).

For the present apparatus, $S \simeq 2$ inches at the hub. The smallest readily available transducers (Kulite CQL-080 series)can be mounted in probes of about 0.10 in diameter, so that $\varepsilon = D/S = 0.060$ at the hub (or 0.040 at the tip). At the design speed of 166 rps, with 23 blades, the frequency response should then be $f > (23)(166)/(.060) = 64$ KHz.

Such high frequency response is difficult to attain with transducers of the above dimensions mounted in any sort of cavity. Consider the stagnation probe design shown in Fig. 7. If the passage is not enlarged at the inner end, adjacent the transducer, this design is limited in

TABLE II

Characteristics of Instrumentation

Quantity measure	Instrument	Range	Frequency Response
Supply Tank p, p_1	Strain-gage transducer	0-15 psia	0-100 Hz
Dump Tank p, p_4	Strain-gage transducer	0-15 psia	0-100 Hz
Rotor inlet p, p_2	Strain-gage transducer	0-15 psia	0-100 Hz
Rotor outlet p, p_3	Strain-gage transducer	0-15 psia	0-100 Hz
Supply temp $T_1(0)$	Thermocouple		D.C.
Supply pressure $p_1(0)$	Bourdon gauge	0-760 mm	D.C.
Flow static p	Kulite in cavity*	0-15 psia	0-50 KHz
Flow stag. p	Kulite in cavity*	0-15 psia	0-17 KHz
Wall stat. p	Kulite exposed	0-15 psia	0-100 KHz
Mass flow density, ρu	const. temp. hot wire	variable	0-20 KHz
Rotor speed	Magnetic pickup on toothed wheel		19,100 Hz at design speed

* see discussion for details

frequency response by resonance at the quarter-wave frequency of the passage, which is $f \simeq a/4\ \ell$. Taking $a \simeq 820$ FtS^{-1}, $\ell \simeq D = .0083$ ft, $f \simeq 24{,}600$ Hz. To reach the size-limited response of 64 KHz, ℓ must be reduced to about D/2, resulting in a probe with very little if any projection of the impact tube beyond the cylindrical body. The probe used in the present tests had the dimensions D = 0.108 in., $\ell \simeq$ 0.15 in. Its cavity resonance frequency, determined by its response to a step pressure change produced by a shock tube, was between 16 and 20 KHz. Steady state tests in a free air jet showed deviation of less than 1 percent from true stagnation pressure for flow angles of $\pm$ 17 degrees from the axis of the impact tube.

Time resolved measurements of the local static pressure in the compressor annulus require a probe which is insensitive to the magnitude of the dynamic pressure, and to the flow direction since it does not seem feasible to develop a probe capable of aligning itself with the local flow on the time scale of blade passing. The design used is shown in Fig. 8. It consists of a small cavity fed by several orifices spaced around the cylindrical surface of the probe. The cavity resonance frequency for this design can be as high as 60 KHz because of the large combined area of the ports. If the orifices are uniformly spaced about the cylinder, the cavity pressure is below the true static pressure, as can be seen from the fact that the probe has a non zero drag. For any given Mach number and Reynolds number, the holes can be distributed in such a way that the cavity assumes the true static pressure. Initially, a probe with eight equally spaced holes was tried. It gave a reading about 10 percent of the dynamic pressure below true static for the Reynolds number range of

interest here. A second design is shown in Fig. 9 along with its fractional error from true static pressure as a function of Reynolds number. The value 0.5×10^5 at which the error rises suddenly is in the range where the drag coefficient for a cylinder drops suddenly due to transition.[2] Up to this Reynolds number, the fractional error in static pressure is less than 0.6 percent, even though the Mach number is as high as 0.6. The range of Reynolds number attained in the experiment is well within the low error range, as shown. The cavity resonance frequency for this probe was found to be 53 KHz.

3.2 Optical Flow Diagnostics

After consideration of a number of shadowgraphic and schlieren techniques, it was concluded that the ray-averaging characteristics of all such conventional visualization techniques made them unsuitable for three dimensional flow visualization. Accordingly, emphasis has been put on the development of techniques which enable true three dimensional visualization. Two such techniques have been developed to the stage where they are ready to be applied to the compressor. Both would utilize the idea of illuminating the inter-blade passage with a thin sheet of light, and viewing light scattered by the gas from this sheet, the scattered light intensity depending on the gas density so that the light sheet forms a two dimensional density map of the flow. By moving the light sheet, the full three dimensional flow would then be mapped.

The two methods differ in the means of production of the density-related scattered light. In one method the gas is seeded with a fog of droplets, and the light scattered from these droplets is detected. In the other, a fluorescent gas is added to the main gas mixture, and the

fluorescent intensity becomes a measure of the gas density.

Both techniques must satisfy the requirement that exposures be made in times of the order of one to ten microseconds, which corresponds to spatial resolutions of 0.3 to 3 mm at the rotor tip speed of 1000 ft/sec $\simeq 3 \times 10^5$ mm/sec.

3.2.1 Light Scattering

Consider first the colloidal scattering technique. The colloidal suspension can be produced in a number of ways; e.g. by combustion of tobacco, or by use of an atomization process. The latter has been selected for use here. The Sinclair-La Mer[3] aerosol generator produces particles of diameters in the range from 0.2 to 0.7 μm with rather small size spread (less than 50 percent) using a low vapor pressure fluid such as pump oil. The concentrations are in the order of 10^{13} cm^{-3}. If visible light is used, the particle size is in the Mie scattering regime, i.e., in the range where $\alpha = 2\pi R/\lambda$ is of order unity, R being the particle radius and λ the wavelength of the light.

The scattered light intensity at a distance L from the scattering volume (per particle) is

$$I_{1,2} = I^o_{1,2} \frac{\lambda^2}{4\pi L^2} i_{1,2}$$

where the subscripts 1,2 refer to polarization vectors perpendicular and parallel to the plane of observation, respectively, and I^o is the intensity of the incident light. The Mie functions i_1 and i_2 depend on the angle of scattering, θ, from the direction of incidence, and on the size parameter α. For $\alpha << 1$, (Raleigh limit) the intensity is independent of θ, and varies as α^6. F or $0.1 < \alpha < 1$, the dependence on α remains, but there is a pronounced minimum in $i_{1,2}$ for right angle scattering. As α is

increased from unity, i_1 and i_2 for a given scattering angle first increase rapidly to values between 10 and 1000, then oscillate in α.

For a distribution of drop sizes, the sensitivity to drop size tends to average out, as does the variation with scattering (viewing) angle. Thus, it was hoped that by using a technique which is self-calibrating, a quantitative measure of density could be obtained in spite of the sensitivity to drop size and viewing angle. It is intended that this be achieved by including in the field of view a region of known density, e.g. just upstream of the rotor. If the droplet size distribution and viewing angle do not change appreciably between this point and the rotor flow passages, the ratio of scattered light intensities at the two points should equal the ratio of particles, which in turn equals the ratio of gas densities.

For particles of the size considered here, slip is not a problem, even shocks being resolved to within a fraction of a millimeter.

This technique was tried in the shock tube experiment shown schematically in Fig. 10. The light source was a commercial spark source collimated to a 1 cm diameter beam. Photographs obtained with Polaroid film (ASA 3000) at f 1.2 are shown in Fig. 11. The top photograph is of the uniform density gas, for calibration. The bottom one shows the shock, advancing from right to left, with a density ratio of 1.5.

Microdensitometer measurements of the lower photograph yielded a density ratio across the shock of 1.5 ± 0.1.

As this shock has roughly the density ratio expected in the transonic rotor, it is concluded that the light scattering technique should be capable of defining at least the stronger shock systems. With further development it should also give information about the more gradual density

changes in the rotor passage, although the beam attenuation shown in Fig. 11 is a problem in this respect.

3.2.2 Gas Fluorescence

This technique has the obvious advantage that it allows use of a gas, and so eliminates the possibilities of particle coagulation, variation in particle size, and viewing angle sensitivity which may occur with the light scattering technique. A more significant advantage may be that the light emitted by the fluorescent substance is at a different wave length than the exciting light, so that reflections from surfaces should be less of a problem. On the other hand, fluorescent intensities are generally rather small, so that the short time resolution poses a serious problem.

An extensive study of the possible fluorescent substances has been made by Epstein, and is reported in his thesis.[4] The conclusion is that one of the most suitable substances is a polymer of acetone (2,3 butanedione, $CH_3CO\ CO\ CH_3$), which is a watery, nontoxic liquid with vapor pressure of 40 torr at ambient pressure. Its fluorescence as a pure substance has been extensively studied.

Study of the literature on butanedione fluorescence showed that in fact, when irradiated by light of wavelength between 3000 and 5000 Å, it fluoresces in the blue (4500 - 4800 Å) from the first excited singlet state with a lifetime of about 10^{-8} sec, and phosphoresces from the first excited triplet state with a much longer lifetime, near 2×10^{-3} sec and in the green (4900 - 6100 Å). The ratio of intensities is 60 to 1, the phosphorescence being more intense.

According to the literature, the phosphorescent intensity is proportional to butanedione pressure. If this is also true when the

butanedione is carried in a background gas, the emitted intensity should, as mentioned above, be a direct measure of gas density. That this is in fact true when butanedione is carried in the argon-freon mixture chosen for the Blowdown Compressor, has been verified by Epstein. His results for phosphorescent intensity as a function of mixture pressure are shown in Fig. 12.

Because the lifetime of the phosphorescence is long compared to the flow time through the compressor, the phosphorescence can be used to produce tracers, much as the hydrogen bubble technique is used in water. It does not seem as suitable for local density measurements.

The short lifetime of the fluorescence allows its use for local density probing, provided sufficient intensity can be obtained.

Epstein concluded from his study of various light sources and imaging techniques that a number of schemes are feasible. In order of preference, they are

1) excitation by a flash tube, and imaging by an image converter camera;
2) excitation by a dye laser and direct photography;
3) excitation by a flash tube, and direct photography (but this requires a 10 μs shutter with large aperture which is difficult to achieve).

Unfortunately, the cost of the equipment for these three alternatives decreases in the same order as their viability.

IV. TEST SECTION AND ROTOR

The test section and compressor stage are designed for a maximum of flexibility and diagnostic ease, in combination with realistic simulation of high Mach number - high pressure ratio compressors. An overhung rotor without inlet guide vanes, with an inlet hub/tip radius ratio of 0.5, a tip tangential Mach number of 1.2, design pressure ratio of 1.6 and radially constant stagnation temperature rise were selected. For the sake of diagnostic ease the casing is cylindrical, all of the rather large area reduction being taken in the hub contour. The hub was made conical, to facilitate its use as a reflector for optical flow visualization.

4.1 Rotor Design

Aside from these features, the rotor is of rather conventional design. For the conditions given above the inlet and outlet air angles relative to the rotor, β_1' and β_2', are as shown in Table III. An aspect ratio of about 2, and tip solidity of unity, were chosen, giving a maximum diffusion factor D = 0.50 at the root, and 23 blades. Fewer blades, and thus lower aspect ratio would have been preferable from the standpoint of minimizing the blade passing frequency, but the blade chords would then have exceeded the capacity of the GTL blade miller. The blade sections were laid out on conical stream surfaces estimated by the method outlined in Appendix A, using double circular arc sections for the subsonic portion of the blade, and multiple circular arc sections for the supersonic portion; with flat suction surfaces faired to circular

arcs so as to put the point of maximum thickness at 2/3 chord. The thickness to chord ratio varies linearly from 0.1 at the hub to 0.03 at the tip, the leading and trailing edge radii from 0.020 inches at the hub to 0.010 at the tip. Blade incidence and camber were selected by the method of Ref.(3), using the correlation presented there for the subsonic portion of the blades. The incidences, i_c, and cambers, as given by this method are shown in Figure (13) as the dashed lines. As the rotor is expected to operate with a supersonic suction side at the tip, the incidence there should be such as to align the flow with the suction side of the blade. The incidences required to satisfy this condition are shown as the second (lower) dashed line in Figure (13). The design incidence was selected as the solid line, giving zero suction side incidence at the tip and agreeing with the correlation at mid-span, where the blade relative Mach number is approximately unity. The camber was adjusted in the supersonic region to the same trailing edge angle as given by the correlation, resulting in the solid line shown in Figure (13). The design values of incidence, i_c, camber, ϕ, leading and trailing edge angles α_1 and α_2, and various other parameters are summarized in Table III for the calculated stream surfaces. The blade cross sections, projected onto the conical streamsurfaces, are shown in Figure (14). The sections were stacked on a radial line through their mid chord points, with the chord angles γ° given in Table III.

The stator has not yet been designed nor fabricated, but the air angles, streamtube radii, and required diffusion factors for a tip solidity of unity are summarized in Table III. Both the stator entrance Mach number and the diffusion factor are reasonable except possibly for the

TABLE III

Design parameters of rotor and stator
for each design streamsurface

r_1/r_T	0.5	0.6	0.7	0.8	0.9	1.0
r_2/r_T	0.64	0.71	0.78	0.85	0.93	1.0
M_T	0.60	0.72	0.84	0.96	1.08	1.20
M_1'	0.78	0.88	0.98	1.07	1.19	1.30
β_1'	50.2	55.2	59.2	62.5	65.2	67.4
β_2'	23.8	35.7	44.2	50.6	55.6	59.5
σ_r	2.00	1.67	1.43	1.25	1.11	1.00
D_r	.50	.49	.45	.43	.40	.38
i_c	11.5	10.4	9.9	7.7	4.5	1.3
ϕ	22.0	14.7	9.0	7.5	6.7	8.1
α_1	38.7	44.8	49.3	55.0	61.2	66.1
α_2	16.7	30.1	40.3	47.5	54.1	58.0
$\gamma°$	28.9	38.1	45.0	51.1	56.3	61.7
t/c	0.10	.086	.072	.058	.044	.030
M_3	.68	.65	.62	.60	.58	.57
β_3	47.5	44.6	42.0	39.4	37.0	35.0
r_4/r_T	0.68	0.74	0.80	0.86	0.93	1.00
σ_s	1.57	1.41	1.28	1.18	1.08	1.00
D_s	0.55	0.53	0.52	0.50	0.48	0.47

hub streamline, where D = 0.55 seems rather high.

4.2 Fabrication of Blades

The rotor blades were milled from aluminum plate in the GTL blade milling machine. This machine works from a blade master four times actual size, feeding the blade stock through a pair of milling cutters, one for roughing and one for finishing, which are controlled through pantographs by wheels rolling on the master. The large size of these blades necessitated scaling the master by a factor of two in the radial direction, rather than four. The master was constructed by mounting aluminum templates of the desired blade shape on a radial spindle at the correct chord angles, then fairing between them with plastic putty. After milling the blades were hand finished with emery cloth to remove the milling marks.

Because of the modest stress levels and absence of high cycle fatigue problems, the blades were mounted with simple pinned butts fitted into slots milled into the rotor rim at the hub chord angle. The completed rotor with spinner and outlet fairing is shown in Figure (15).

4.3 Rotating Assembly

The rotor shaft, speed monitoring and electric motor drive assembly are shown in Figure (16). This system posed two unusual problems, that of operating the bearings within the vacuum system, and that of sealing. To avoid the difficulties of motor operation at low pressures, the motor was placed in a chamber at atmospheric pressure, driving the main spindle through a 1/2 inch diameter shaft, on which the seal is mounted. This arrangement lowers the seal rubbing velocity to a level tolerable

for a commercial oil-pressurized graphite face seal.

The bearings are ABEC-7 angular contact type, two in tandem at the rotor end, and one spring loaded in opposition at the other end of the shaft. They are grease packed, thus eliminating problems of contamination from lubricating oil. Initially, the front two bearings were installed as a duplex pair, to provide for thrust capacity in either direction during the transient blowdown. In this configuration the bearings heated and failed. The configuration shown allows the two front bearings to share the forward thrust of the rotor during normal operation, but any rearward thrust which may occur during the first few milliseconds of blowdown must be taken on the axial loading spring. This has caused no trouble so far.

The critical speed of the hub, spinner and shaft assembly was estimated at 400 Hz, neglecting bearing deflections. As this is well above the design speed (166 Hz) no difficulty was expected from this source. The drive motor is a 24 volt 300 amp surplus aircraft generator, designed for 9 kilowatt output. It is operated with lower field current and higher than rated armature voltage, to overspeed it to the desired 10,000 rpm at the design point.

Speed measurement is by two magnetic pickups, one excited by the teeth of a 115 tooth gear, the other by a single insert in the gear, to give both a once-per-revolution index pulse, and a 115 per revolution speed signal.

4.4 Stator Hub

The stator hub fairing shown in Figure (16), fabricated of aluminum,

is demountable. It is intended that it be replaced by a series of rings, one of which will support the stator blades. This arrangement avoids the problem of penetrating the vacuum shell of the test section with many stator supports.

4.5 Instrumentation Ports

A series of 1/2 inch diameter instrumentation ports are provided on one side of the test section at the locations shown. On the other side, a demountable 6 x 18 inch plate is provided for optical access. This plate is machined to the casing contour on the inside, and has been provided with a 5 inch diameter quartz window with a matching inner contour, i.e., a negative cylindrical lens.

V. PRELIMINARY EXPERIMENTS

In the preliminary experiments to be described here, the emphasis has been on assessing the viability of the blowdown compressor as a test facility, rather than on detailed investigation of any particular aspect of the rotor's behavior or performance. It was just that such a verification of the basic testing concept was of prime importance, in view of its novelty.

A long series of experiments was carried out, using air as the test gas, in the course of initial facility checkout and diaphragm development. These will not be described, as their culmination is completely summarized in a single experiment, carried out with the Argon-Freon 12 mixture, but without the compressor rotor. This test (No. 49) will be discussed in some detail as a gas-dynamic checkout of the facility.

A series of experiments was carried out with the rotor in place. Their features are tabulated in Table IV. One, No. 47, was carried out at half speed. Four others, 48, 50, 51 and 52 were at design speed, with different throttle plate diameters, and varying types of instrumentation as indicated in Table IV.

5.1 Gasdynamic Checkout Without Rotor

The pressures in the supply tank (p_1), ahead of the rotor and spinner (p_2), in the annulus position downstream of the rotor (p_3) and in the dump tank (p_4), are shown in Fig. 17 for an experiment carried out with the spinner and rotor removed. The stagnation pressure was also measured in the downstream annulus, by the probe described in section IV, traversed across the annulus in about 20 milliseconds some 60 milliseconds after diaphragm firing.

TABLE IV

Conditions, Instrumentation and Features
of Preliminary Experiments

Experiment No.	47	48	49	50	51	52
Supply press., mm	502	489	483	496	495	495
Rotor speed, rps	82.5	170	No rotor	170	170	170
Throttle plate diameter, in.	17.60	17.60	17.60	17.40	17.20	17.20
Instrumentation:						
Hot wires	Sta.2,3	Sta.3	—	—		
Static pressure	—	—	Sta.2	Sta.2	Sta.2	Sta.2
Stag. pressure	—	—	Sta.3	Sta.3	—	Sta.3
Features	oscilla-tions	2-cell stall	gas dynam. checkout	1-cell stall	design-point operation	

We note first of all that there is an initial period of about 95 milliseconds during which the flow is distinctly unsteady in character, with p_2 and p_3 initially rising above the supply pressure, p_1, then oscillating. These fluctuations are associated with the filling of the cavity between the diaphram and throttle plate, and are of course to be expected. They appear to settle down enough by 95 milliseconds to allow rotor testing at normal speeds, although the oscillations are a problem for low speed (low pressure ratio) tests, as will be seen below.

5.1.1 Mass Flow Determination

There are at least three methods by which the compressor mass flow can be determined in this experiment. These utilize:

1) the rate of change of pressure (density) in the supply tank. The mass flow rate is

$$W = \frac{V_1}{(1 + \delta)a_1^2(0)} \left[\frac{T_1(0)}{T_1}\right] \frac{dp_1}{dt} \qquad (5.1)$$

where δ is the fraction of total flow diverted by the boundary layer scoop, $a_1(0)$ is the speed of sound in the supply tank before firing, and $T_1(0)$ is the corresponding temperature. The boundary layer bypass choking orifice was adjusted in early tests to give a pressure in the bypass duct equal to that in the compressor inlet, and the value of δ was then calculated to be 0.1. Note that even 10 percent error in δ then results in only 1 percent error in W;

2) calculation of M_2 from p_2 and p_1 by the assumption that $p_{t2} = p_1$. This leads to the relation,

$$W = \frac{\gamma p_2 A_2}{a_1(0)} \sqrt{\frac{2}{\gamma-1} \left[\frac{T_1(0)}{T_1}\right] \left(\frac{p_1}{p_2}\right)^{\frac{\gamma-1}{\gamma}} \left[\left(\frac{p_1}{p_2}\right)^{\frac{\gamma-1}{\gamma}} - 1\right]} \tag{5.2}$$

3) calculation of the mass flow through the (choked) throttle orifice, using the measured value of p_3. This gives

$$W = \frac{\gamma p_3 A_t}{a_3} \left[\left(\frac{2}{\gamma+1}\right)\left(1 + \frac{\gamma-1}{2} M_3^2\right)\right]^{\frac{\gamma+1}{2(\gamma-1)}} \tag{5.3}$$

where M_3 is determined by the ratio A_t/A_3 and a_3 is given with adequate precision by,

$$a_3 = a_1(0)\left[p_3/p_1(0)\right]^{\frac{\gamma-1}{2\gamma}}$$

This method would certainly be most precise except for the effect of rotor-exit swirl on the orifice flow.

The mass flow was calculated from the data of Fig. 17 by all three methods, at the time indicated on the figure, and also by applying method 2 at station 3. Comparison of this latter result to that from Eq. (5.3) indicated that the throttle plate has an effective area 0.94 times its geometrical area, a reasonable value. The corresponding values of M_3 and M_2 are $M_3 = 0.44$, and $M_2 = 0.24$. The latter agrees with the value of $M_2 = 0.26$ inferred from the ratio p_2/p_1. For this experiment, method 1 also gave a mass flow within 1 percent of the value from method 3, using $\delta = 0.1$ and $V_1 = 4.34\ m^3$. This method has however the drawback that it requires differentiating the supply pressure as a function of time.

From these several results, it is concluded that the most reliable method of mass flow measurement is the choked downstream orifice. With the addition of straightening vanes and a short plenum, its precision

could be maintained in the presence of rotor-exit swirl.

5.1.2 Test Time

The available test time may be regarded as the time between cessation of the initial oscillations, and the time when the outlet orifice unchokes. Taking the latter as the time when p_1 is 1.89 times p_4, the test time is 0.16 - 0.09 = 0.07 seconds. As the rotational period at design speed is about .006 seconds, the test time allows for some ten complete revolutions of the rotor at constant Mach number. This time is influenced somewhat by the rotor, as will become clear later.

5.2 Half-Speed Experiment

The principal results of an experiment at approximately one half design speed (82.5 rps) are presented in Figs. 18 - 21. Referring first to Fig. 18 we see that the rotor tangential Mach number varied slightly from 0.72, compared to the design value of 1.2. In order that the rotor velocity triangles be near design, the axial velocity must be reduced correspondingly. With the fixed exit orifice area, the exit axial Mach number decreases as the orifice unchokes, so that a "match point" occurs at one time during the blowdown, as indicated on Fig. 18 at t = 0.234 seconds.

Variations of stagnation temperature, T, and the square of rotor speed, with time, are shown in Fig. 19, the temperature being calculated from the p_1 variation of Fig. 18. The rotor speed computed from the time signal generated by the rotor mounted magnetic pickup, first increases slightly, then falls. The initial increase is evidently due to the rotors windmilling as the cavity behind it fills in the initial transient. Even after this initial transient, the rotor slows less rapidly than would lead to constant

Mach number operation, because the axial Mach number is larger than that required for velocity triangles similar to those at design, and the rotor work is correspondingly less. This is indicated by the comparison of $[\omega/\omega(0)]^2$ and $T_1/T_1(0)$, normalized to unity at t = 0.13 seconds.

The ratio p_{3T}/p_2 is shown during the entire blowdown in Fig. 20. Here the subscript T denotes that the static pressure p_{3T} is measured at the casing. We see that $p_{3T}/p_2 < 1$ during the time when the rotor accelerates. It then oscillates about unity with a period approximately equal to the half-wave period of the supply tank, the oscillation gradually damping out and the mean pressure ratio increasing. After the exit orifice unchokes, the pressure ratio rises due to the rising dump tank pressure, and reaches a value of 1.12 at the "match point". Taking the temperature rise across the rotor to be proportional to M_T^2, we would expect a stagnation pressure ratio of 1.18 at the match point, so the static pressure ratio of 1.12 is reasonable.

It appears that the oscillation in the supply tank poses a serious problem for measurements at low rotor speeds, since the rotor does not achieve a steady state lasting for several rotational periods. The behavior might be more favorable with an exit orifice properly matched for the low speed operation. In any case, some useful information can be obtained, as the flow is essentially steady on the blade passing time scale, the oscillation causing the rotor to scan through a range of operating conditions.

Constant-temperature hot wire measurements upstream and downstream of the rotor are shown in Fig. 21, both on the blowdown time scale and the latter also on an expanded time scale which shows the rotor wakes.

Both wires were at midspan. There is a negative signal as the hot explosion products pass over the wires, then a reasonably steady mass flow until past the match point, where the rotor evidently stalls. On the lowest (expanded) time scale each blade wake can be identified prior to and near the match point. As the dump tank pressure rises, the wakes become larger and less periodic, indicating incipient stall.

5.3 Design-Speed Experiments

A series of experiments was conducted at design speed, the exit orifice area being increased in each successive test. In the first tests of this sequence the rotor evidently operated in rotating stall. Some typical information from these stalled cases will be discussed first, to indicate the type of information which can be obtained from the experiment.

5.3.1 Mach Number Matching

The variations of supply tank pressure p_1 and the corresponding T_1, are compared to the variation of rotor speed squared, for Run 48 at design speed, in Fig. 22. There is a slight mismatch during the initial transient, but during the test time, $[\omega/\omega(0)]^2$ equals $T_1/T_1(0)$ within one percent. Thus, the rotor is nearly exactly tailored to run at constant Mach number for an initial pressure of 489 mm Hg.

5.3.2 Operation in Rotating Stall

Hot wire traces ahead of and behind the rotor are shown in Fig. 23 for a test with exit orifice plate diameter of 17.60 inches. Both wire signals show the stall cells, though they are much clearer in the downstream flow. The downstream signal is also shown on an expanded time scale so that the details of one stall cell can be seen, including the individual blade wakes. The stall period is about .006

seconds, very near the rotational period. If the stall propagated at about one half rotor speed, it must have had two cells. Of course, three cells at one third rotor speed would also yield this period.

It should be noted that the stall appears quite periodic over the useful test time (from 0.07 to 0.15 seconds) so that the Blowdown Facility is useful for investigations of stalled behavior.

At the bottom of Fig. 23, the static pressure at the casing downstream of the rotor is shown. It is periodic, with the same period as the stall cells, and it is interesting to note that the pressure is high in the stalled regions.

Decreasing the orifice plate diameter to 17.40 inches resulted in an increase of the stall period to 0.0113 seconds. The static pressure ahead of the rotor, at the casing, is shown on three different time scales for this condition (Run 50) in Fig. 24. At the top is the pressure on the blowdown time scale, obtained from a conventional strain gage transducer. Below this is the signal from a miniature semiconducting strain gage transducer (Kulite) on an expanded time scale showing the pressure signature of the stall pattern, and each blade. A further expansion of the time scale at the bottom shows the pressure pattern in the shock waves running ahead of the rotor.

Note that pressure increases downward in all of these traces. The blade shocks show as abrupt downward spikes on the oscilloscope trace, followed by expansion fans. The time response for the transducer and tape recorder is such as to resolve the twentieth harmonic of the blade passing frequency.

From the oscilloscope trace, it can be seen that the shocks become less sharp in the stall cell. It would seem that a stall signature

as distinctive as this could be identified rather easily.

5.3.3 Unstalled Behavior

Upon decreasing the exit orifice plate diameter to 17.20 inches, the rotor operated unstalled. The supply tank pressure (p_1), static pressure upstream of the rotor (p_2), static pressure downstream of the rotor at the casing (p_{3T}), and dump tank pressure are plotted in Fig. 25. In this test, the downstream stagnation pressure was surveyed by traversing the stagnation probe described in Section IV across the annulus. The position of the probe is shown as a function of time in Fig. 25.

Several points become clear upon comparison of Figs. 17 and 25. First, the mass flow is increased by the rotors pumping, resulting in a more rapid decay of p_1. Secondly, because of this the time at which the exit orifice unchokes occurs sooner, if this time is based on the ratio of supply tank to dump tank pressures. In order to ensure true constant Mach number operation, this must be the criterion, rather than exit orifice choking, in order that the boundary layer bypass flow be a fixed fraction of the total. The net result of these changes is that the available test time extends from about 0.080 to 0.120 seconds, rather than from 0.090 to 0.160 seconds without the rotor. Nevertheless, the test time of .040 seconds is more than adequate for essentially steady state testing, as it corresponds to seven rotational periods. Unfortunately, this shift in test time was not anticipated, however, the probe traverse being timed to occur toward the end of the test time given by Fig. 17, with the result that the measurement of rotor outlet stagnation pressure and efficiency is a bit confused by non-constancy of the boundary layer bypass flow. This situation will of course be rectified in

future tests.

Near the end of the test, we note that the downstream annulus pressure, p_{3T}, approaches the dump tank pressure, p_4, while the rotor upstream and supply tank pressures equalize at a different pressure. This is because the rotor is still spinning, producing a zero-flow pressure ratio of 1.33.

5.3.3.1 Mass Flow and Mach Numbers

The parameters listed in Table V have been calculated for t = 0.140 seconds, when the traversing probe was at about mid span. Mass flow determinations from the exit orifice and from the rate of change of the supply tank pressure check very well. The inlet Mach numbers calculated from this mass flow and the flow areas, are 0.35 ahead of the spinner, and 0.50 at the compressor face. The latter agrees with the design value of 0.50. The tangential Mach number, M_T, was also on design at 1.20. As the rotor design was for constant axial velocity, the downstream axial Mach number should be reduced from the inlet value of 0.5 by the ratio of sound speeds across the rotor. For the measured static pressure ratio of 1.47, the downstream Mach number would be .473, which compares well with the measured value of 0.47. Thus, it appears the rotor operated on design as far as the tangential, inlet, and outlet axial Mach numbers are concerned.

5.3.3.2 Stagnation Pressure Ratio and Rotor Efficiency

The stagnation pressure recorded by the traversing probe, as it scanned from the tip to the hub, is shown in Fig. 26 along with the inlet stagnation pressure, p_1, which of course decreased somewhat during the traverse. The stagnation pressure ratio is also given as a function of radius. Although the peak value of pressure ratio, at about mid radius,

TABLE V

Rotor Performance Unstalled at Design Speed

Parameter	Design Value	Measured
Mass flow (kgs^{-1})	—	12.7 (Eq.5-3) 12.6 (Eq.5-1)
M_2	0.35	0.35 (Eq.5-2)
M_2'	0.50	0.50
M_T	1.20	1.20
M_3	0.50	0.47
$\overline{P}_{t3}/P_{t1}$	1.60	1.52
η_r	—	0.91

is 1.66, compared to the design value of 1.60, substantial regions of lower pressure ratio near the hub and tip lead to an average pressure ratio $\bar{p}_{t3}/p_1 \simeq 1.52$.

From the rotor time signal, a rate of deceleration $d\omega/dt = 808$ rad/sec^2 was inferred, the angular velocity being 139.8 rad/sec. The moment of inertia of the rotor is 0.215 lb ft sec^2. The rotor power is then $P = I\omega d\omega/dt = 207$ kw. The rotor efficiency is $\eta_r = 0.91$.

5.3.3.3 Upstream Rotor Shocks

Throughout this experiment the upstream high-frequency response pressure transducer indicated a periodic signal of the type shown on an expanded time scale in Fig. 27. The amplitude, approximately 0.05 atm, is about 20 percent of the static pressure in the compressor inlet. The shock and following expansion wave from each blade are clearly seen, and quite uniform from one blade to another. It appears that the very high frequency jumps in the trace are due to electrical noise, as they are beyond the frequency response of the transducer.

VI. CONCLUSIONS AND RECOMMENDATIONS

The main conclusion to be drawn from the above information is that the Blowdown Compressor Facility is both viable and practical as a means for aerodynamic testing of transonic compressor rotors. The experimental results, though preliminary and incomplete, demonstrate the feasibility of obtaining quantitative data on the performance of a high Reynolds number, high Mach number compressor rotor by a wide variety of types of instrumentation. Both the usual "steady state" performance of the rotor and the details of unsteady flow due to blade passing and stall can be examined. It is believed that both the cost and time required to obtain these results via the blowdown method have been much less than would have been required by conventional steady state techniques.

Much work remains, however, in the development of techniques of instrumentation, data acquisition and reduction tailored to the specific requirements of the Blowdown Facility. Some progress has been made in each area. High frequency response pressure measurements have been shown to be feasible, but the probes require further development. Optical techniques for direct density measurement in three dimensional flow fields have been demonstrated in small experiments, and must now be applied to the compressor. Data acquisition on a wide-band tape recorder has proven feasible, but data reduction techniques require further development.

It is believed that further development along these lines will lead to a capability for much more detailed examination of the flow in compressor stages than has been possible in the past.

APPENDIX A

STREAM-SURFACE CALCULATION

The location of stream surfaces as they pass through the rotor and stator has been estimated by a simple radial-equilibrium technique, as follows. Conservation of mass flow between the casing and the stream surface with radius r_1 upstream and r_2 downstream of a blade row requires

$$\int_{r_1}^{r_T} \rho_1 w_1 r dr = \int_{r_2}^{r_T} \rho_2 w_2 r dr \qquad \text{(A-1)}$$

where for the rotor ρ_1 and w_1 are constant. Radial equilibrium at station 2 requires $(r/\rho)(d\rho/dr) = M_\theta^2$, where M is the tangential Mach number at station 2. The Euler equation gives $M_\theta = [(1 + \frac{\gamma-1}{2} M_1^2)(\tau_c - 1)/(\gamma-1)M_T](r_T/r)$ where $\tau_c = T_{t2}/T_{t1}$ and M_T is the tip tangential Mach number. Integrating $d\rho/dr$ from r to r_T results in

$$\frac{\rho_2}{\rho_T} = e^{-\varepsilon[(r_T/r_2)^2 - 1]} \qquad \text{(A-2)}$$

where

$$\varepsilon = \frac{1}{2}\left[\frac{(1 + \frac{\gamma-1}{2} M_1^2)(\tau_c - 1)}{(\gamma-1)M_T}\right]^2 \qquad \text{(A-3)}$$

For the cases of interest here, $\varepsilon \ll 1$, so that the exponential form may be expanded to $\rho_2/\rho_T = 1 - \varepsilon[(r_T/r_2)^2 - 1]$. Integrating equation (A-1) with the assumption that $w_2 = w_1 =$ constant then gives

$$\frac{\rho_1}{2\rho_T}\left[1 - \left(\frac{r_1}{r_T}\right)^2\right] = \frac{1+\varepsilon}{2}\left[1 - (r_2/r_T)^2\right] - \varepsilon \log\left(\frac{r_T}{r_2}\right) \qquad \text{(A-4)}$$

A second condition which must be satisfied is that, for isentropic flow,

ρ_T is connected to the stagnation pressure and Mach number downstream of the rotor. Thus, if M is the total outlet Mach number, $M_2^2 = M_{\theta T}^2 + M_1^2/\tau_c = 2\varepsilon + M_1^2/\tau_c$, and

$$\frac{\rho_T}{\rho_1} = \left(\tau_c \frac{1 + \frac{\gamma-1}{2} M_1^2}{1 + \frac{\gamma-1}{2} M_2^2} \right)^{\frac{1}{\gamma-1}} \qquad \text{(A-5)}$$

The right side of eq. (A-4) is plotted versus r_2/r_T for representative values of ε in Fig. A-1. To find r_2/r_T, given r_1/r_T and ε, one computes ρ_T/ρ_1 from eq.(A-5), then computes the left side of eq.(A-4), and reads r_2/r_T off Fig. A-1.

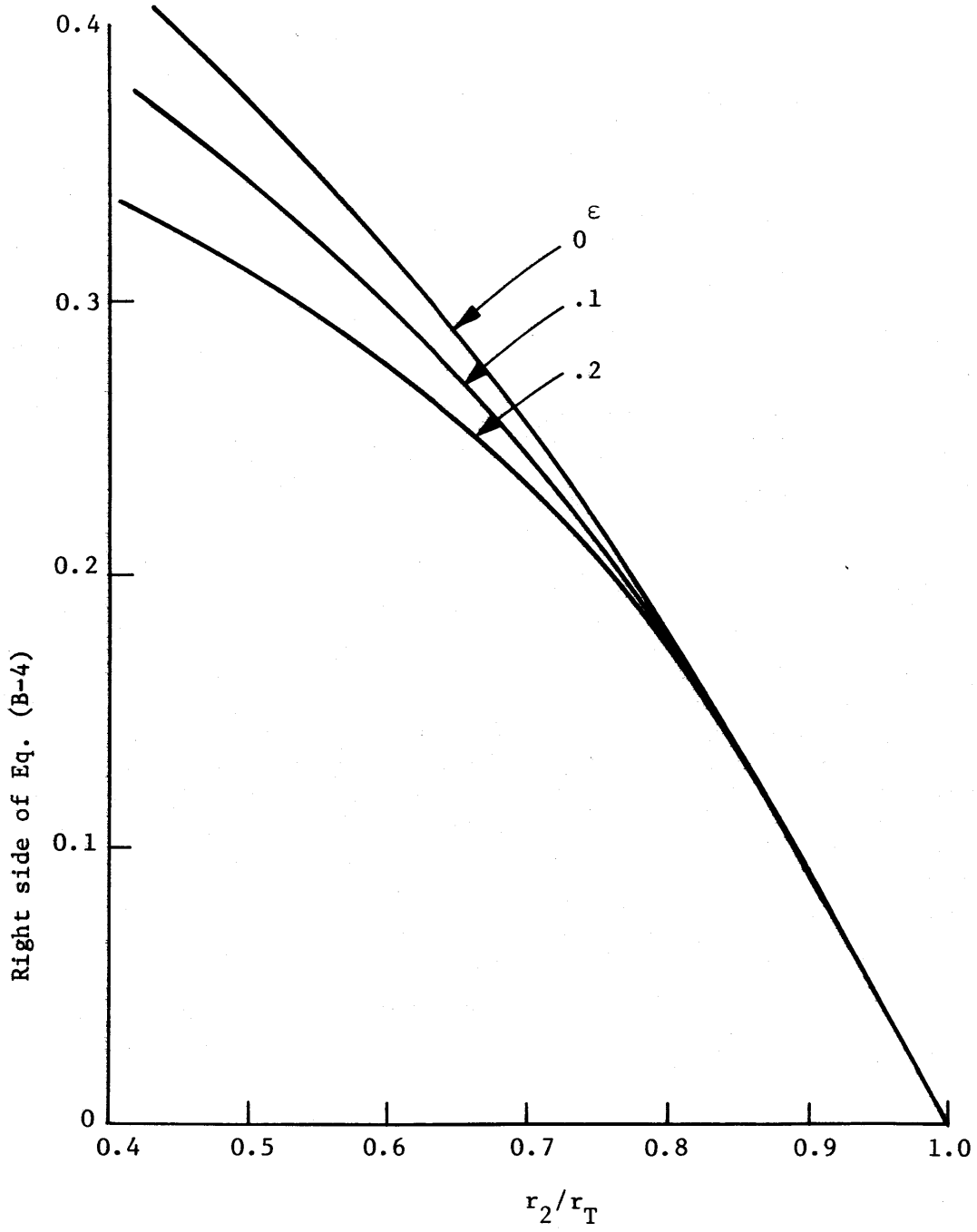

Figure A-1: Right-hand side of Eq. (A-4) as a function of ε and exit streamtube radius ratio.

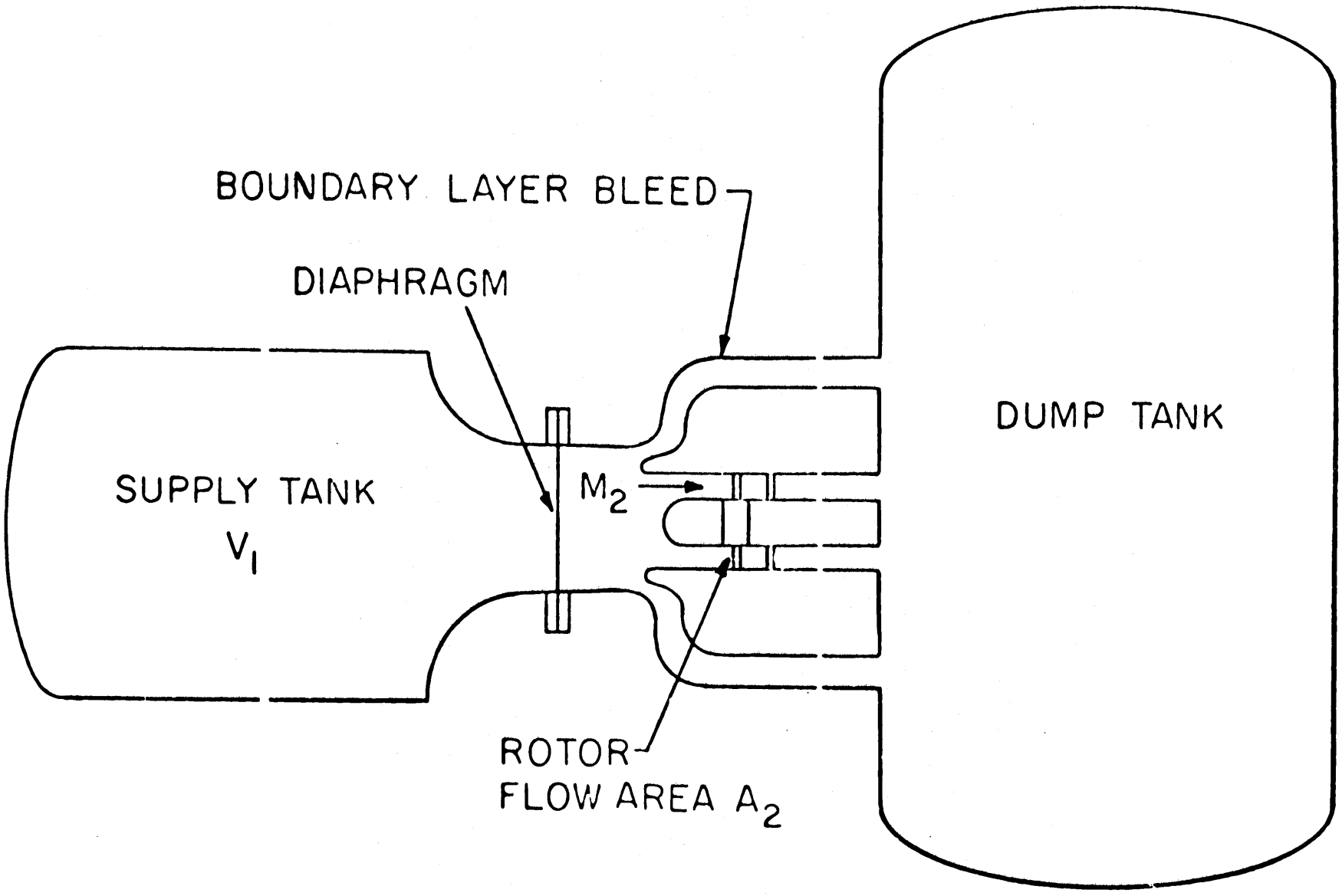

Figure 1: Schematic of Blowdown Compressor Facility, showing supply and dump tanks, diaphragm and boundary bleed which removes flow disrupted by diaphragm, and rotor with inlet flow area A_2.

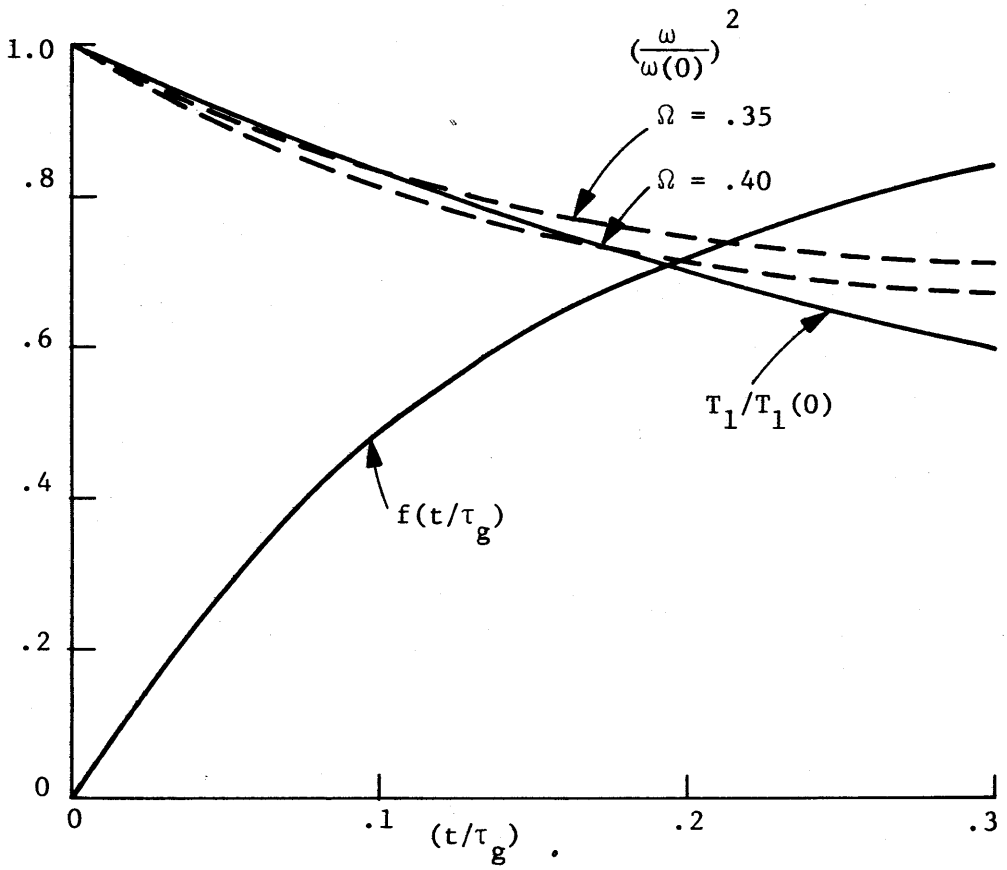

Figure 2

Comparison of the change of the square of the angular velocity of a decelerating rotor to the change in stagnation temperature during the blowdown. The function $f(t/\tau_g)$ is defined above [Eq. (2.6)].

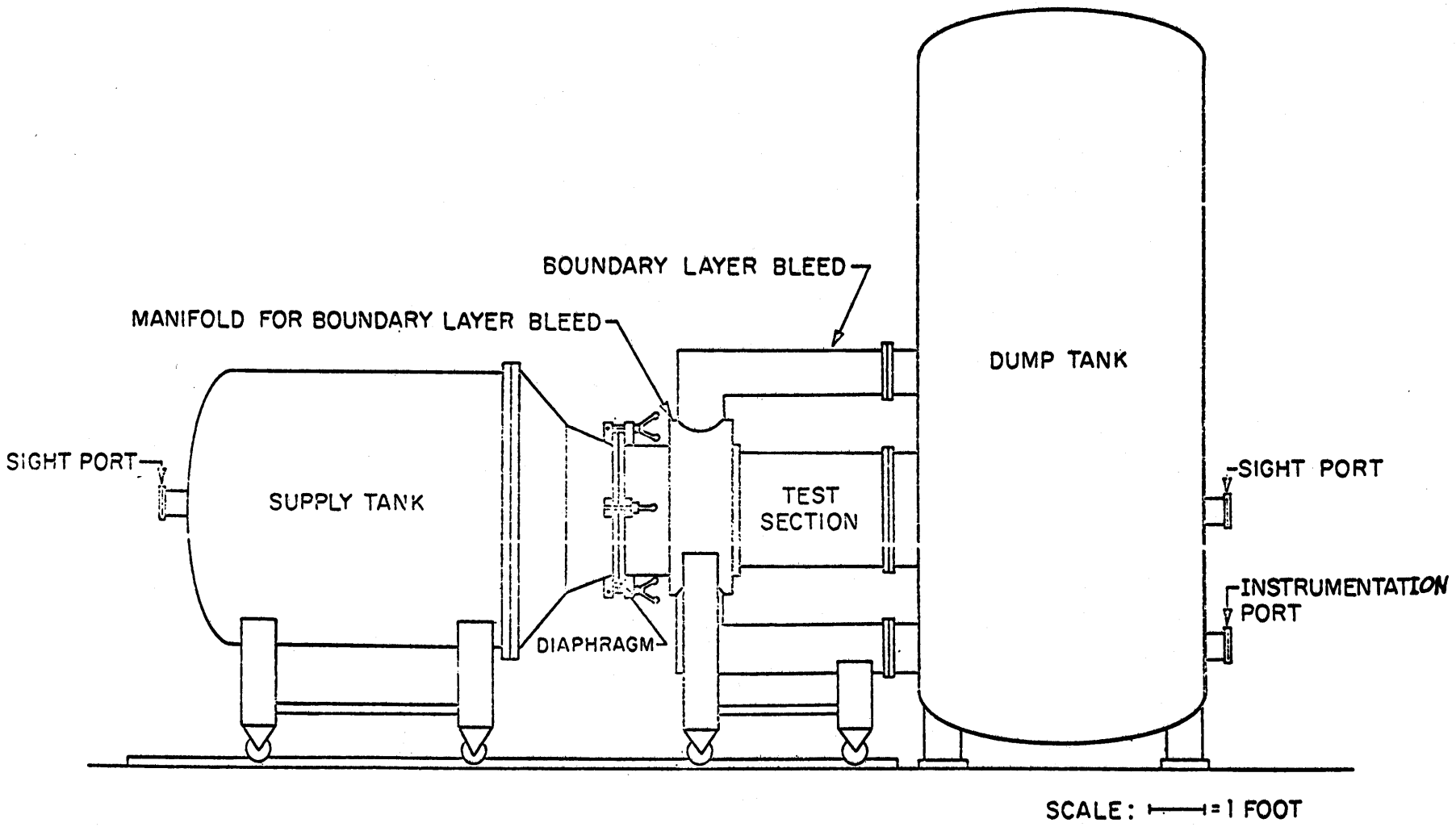

Figure 3: Scale drawing of Blowdown Compressor Facility, sized for 23.25 inch diameter rotor.

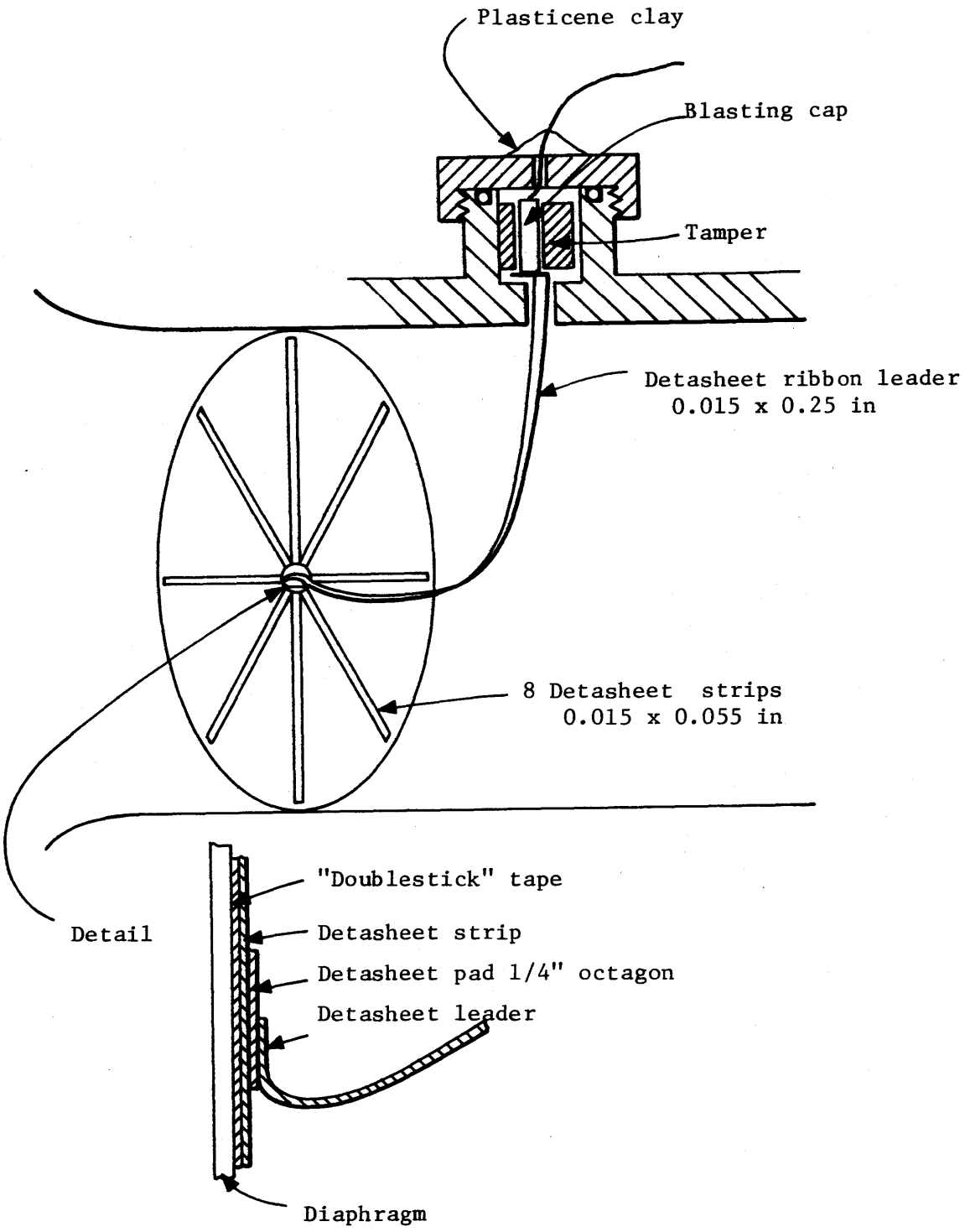

Figure 4

Schematic drawing of explosive diaphragm cutting method.

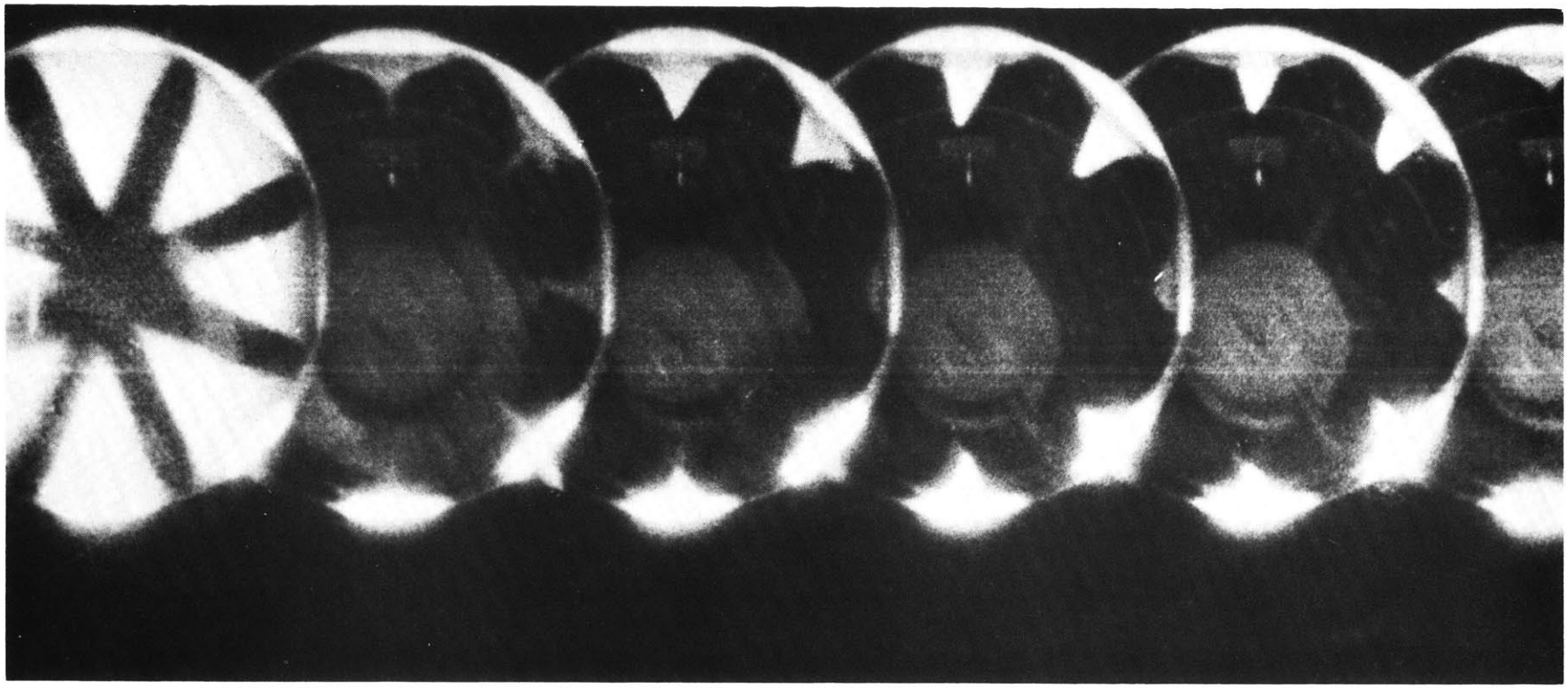

Figure 5: A sequence of frames from a high speed movie of the diaphragm opening sequence. Interval between frames is 1/750 sec.

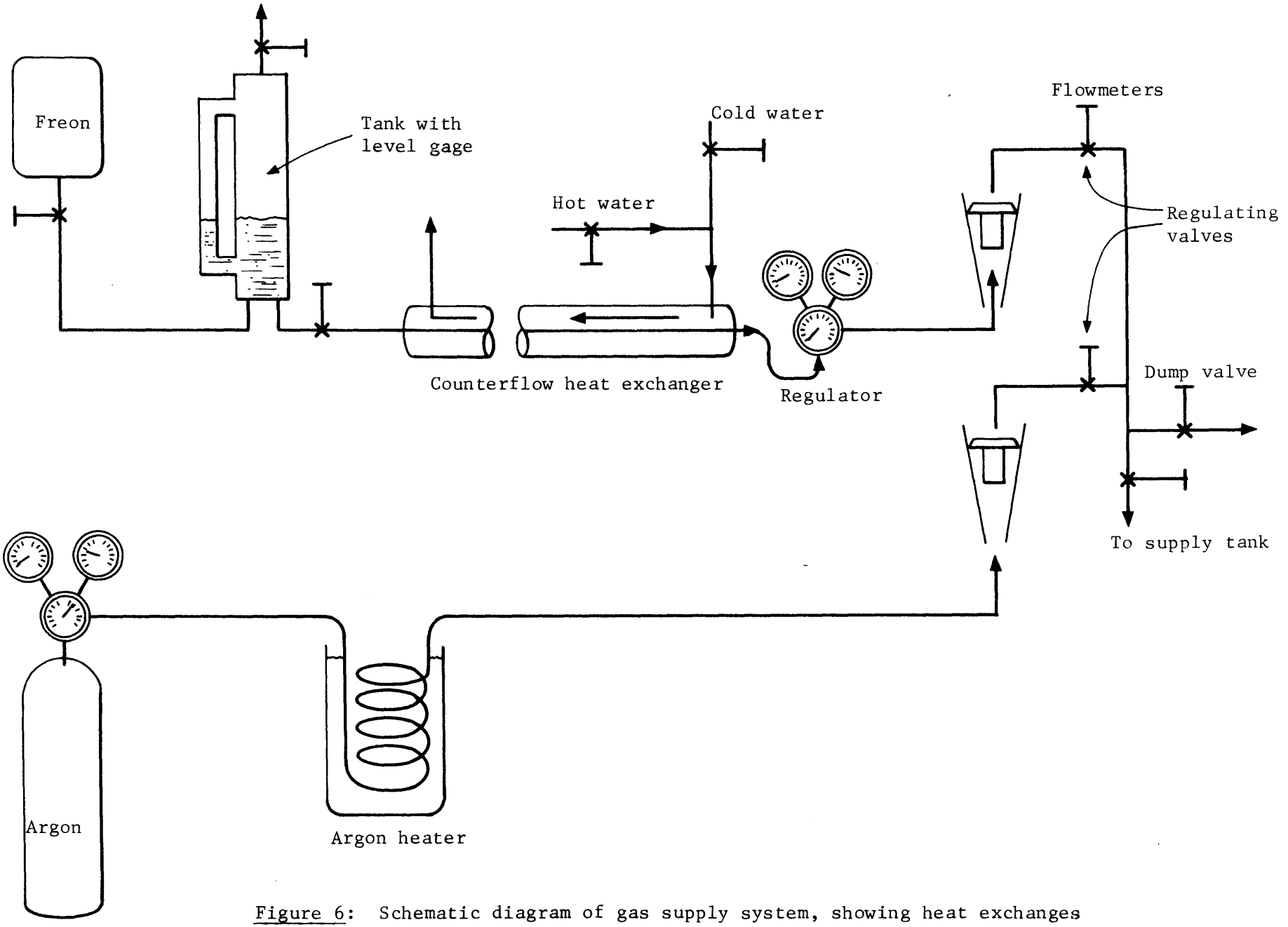

Figure 6: Schematic diagram of gas supply system, showing heat exchanges for boiling Freon, and heater for controlling Argon temperatures regulators and flow meters.

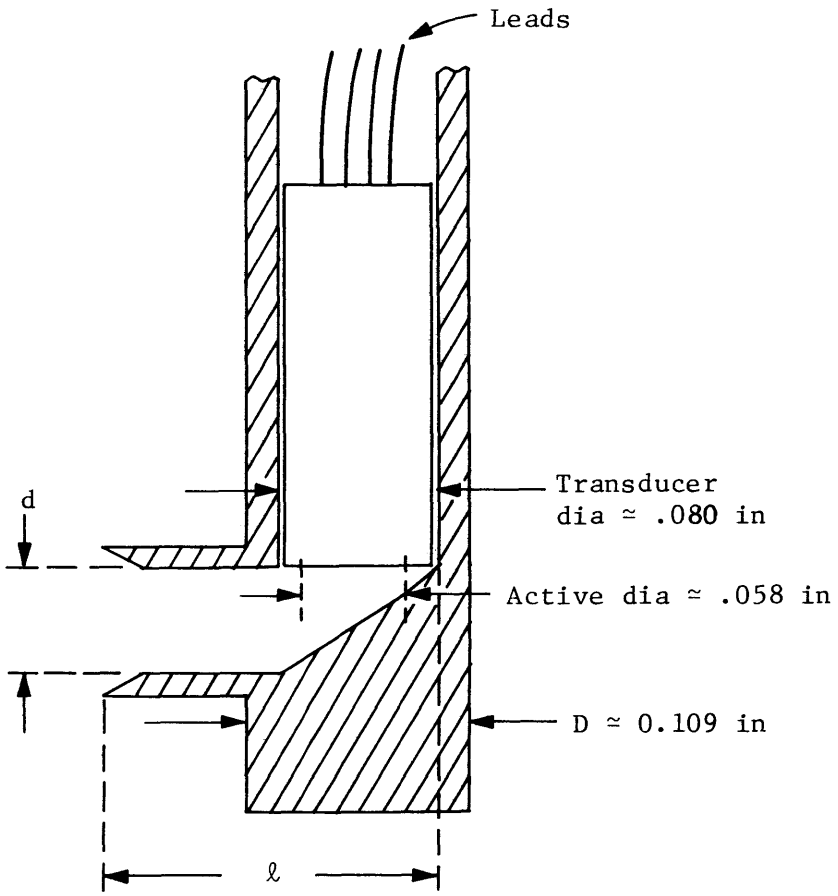

Figure 7

Stagnation pressure probe incorporating semiconducting - strain-gage pressure transducer.

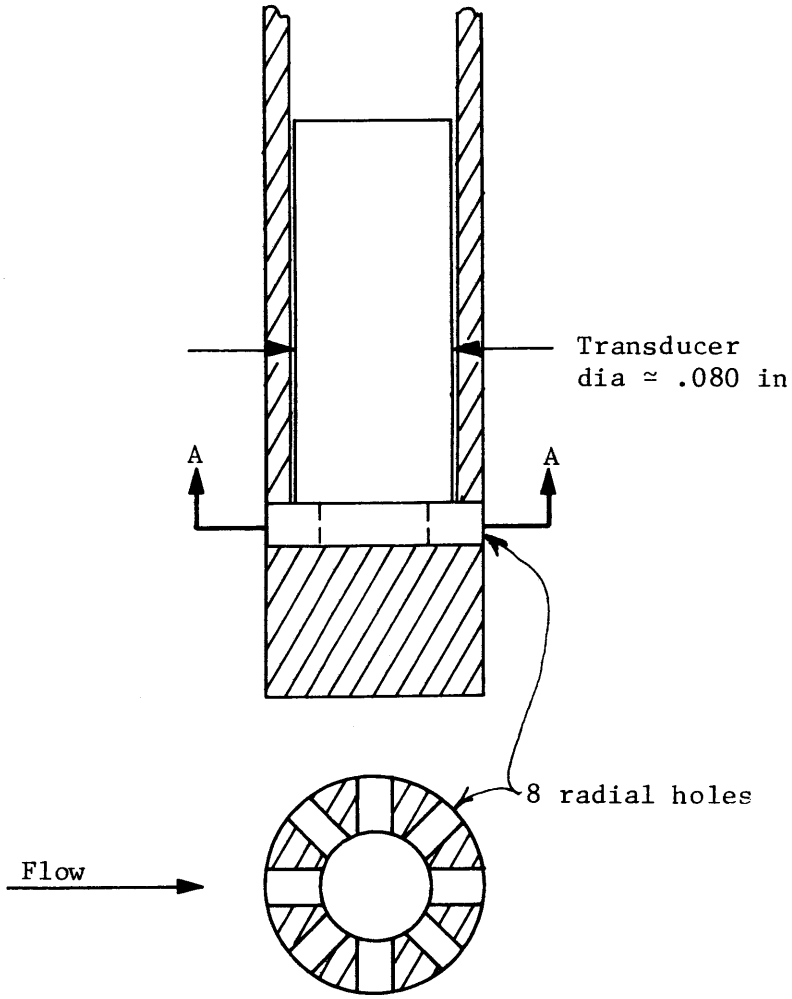

Figure 8

Static pressure probe incorporating semiconducting-strain-gage pressure transducer.

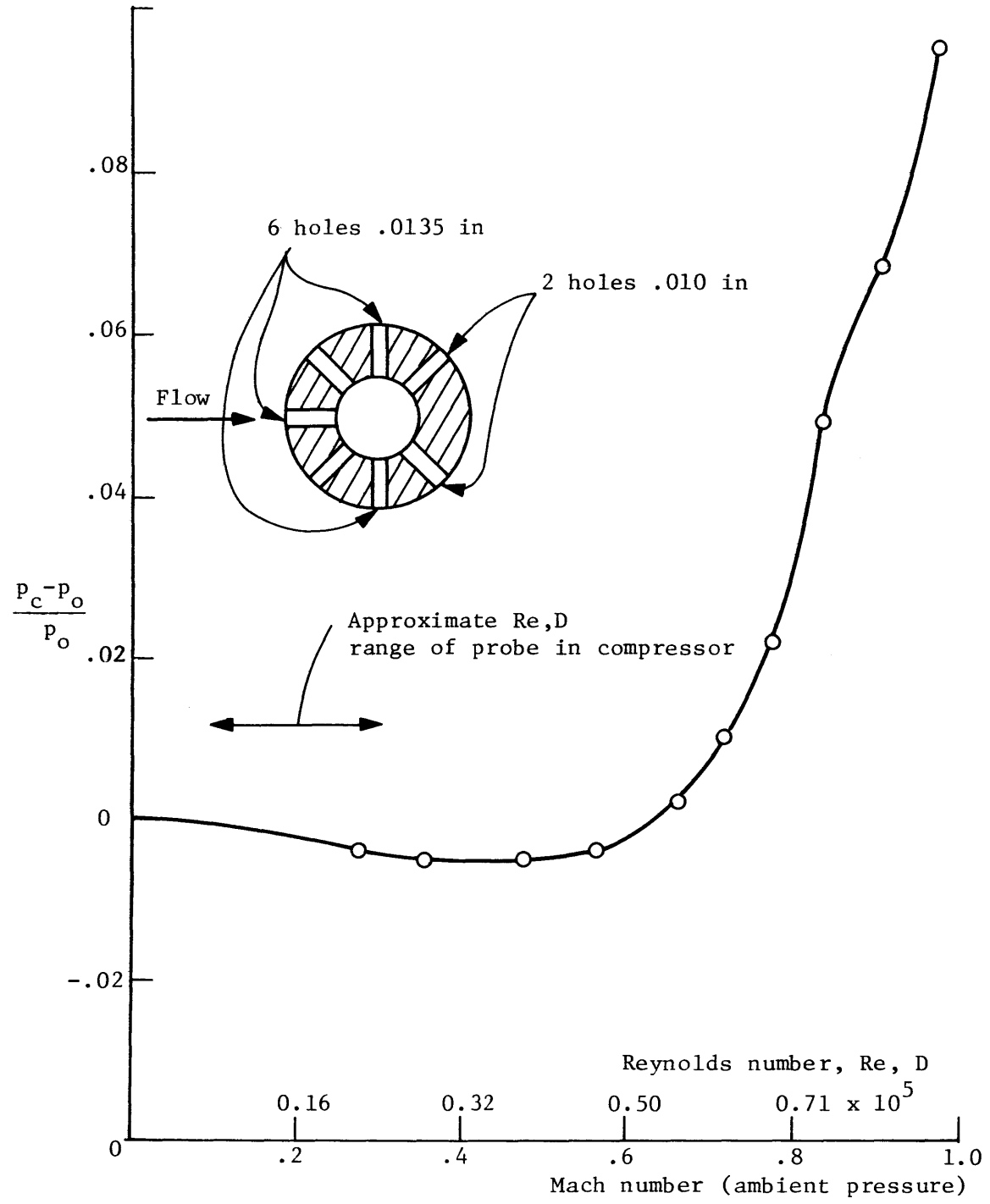

Figure 9: Fractional error in static pressure probe measurement as a function of Reynolds number.

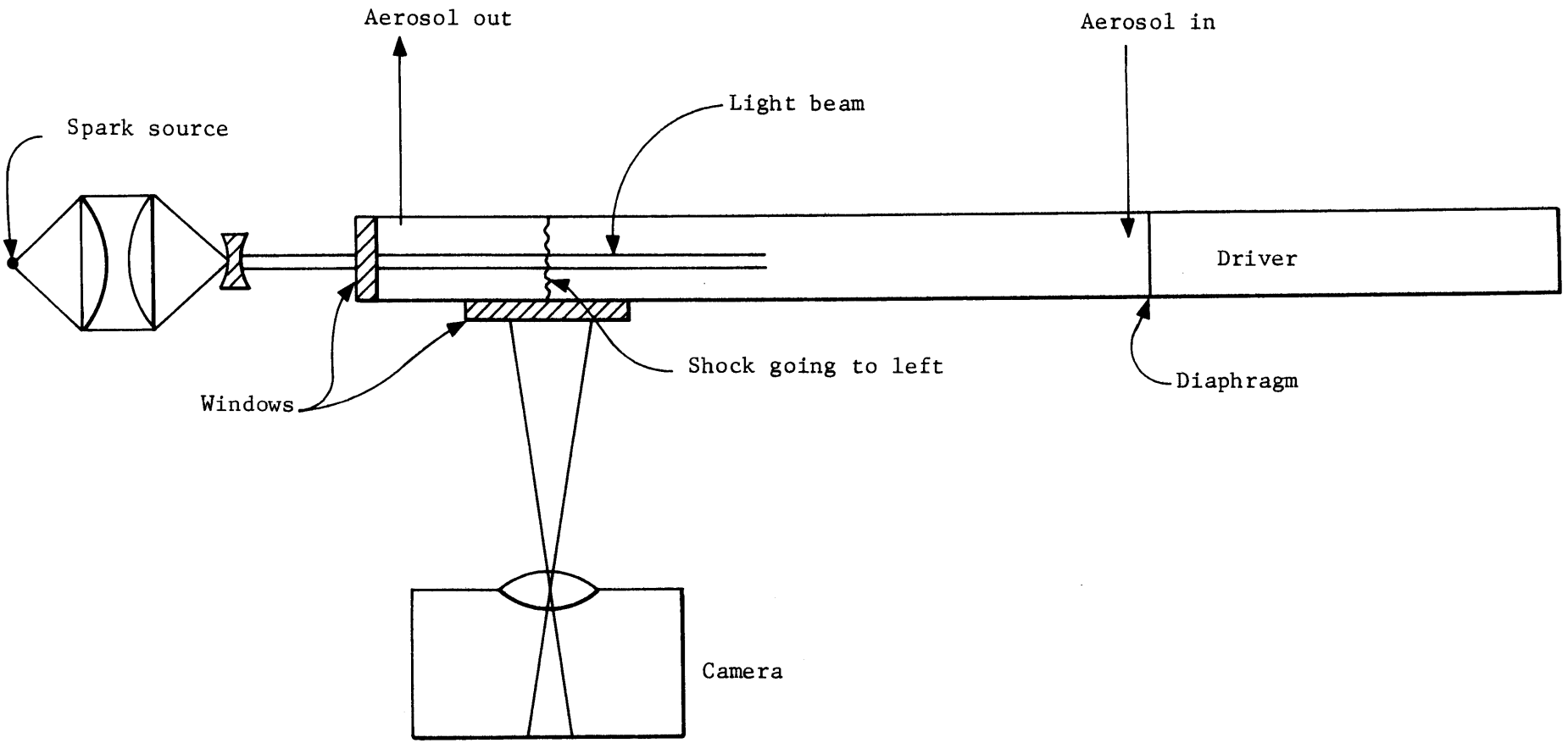

Figure 10: Schematic of setup for photographing shock by light scattered from aerosol.

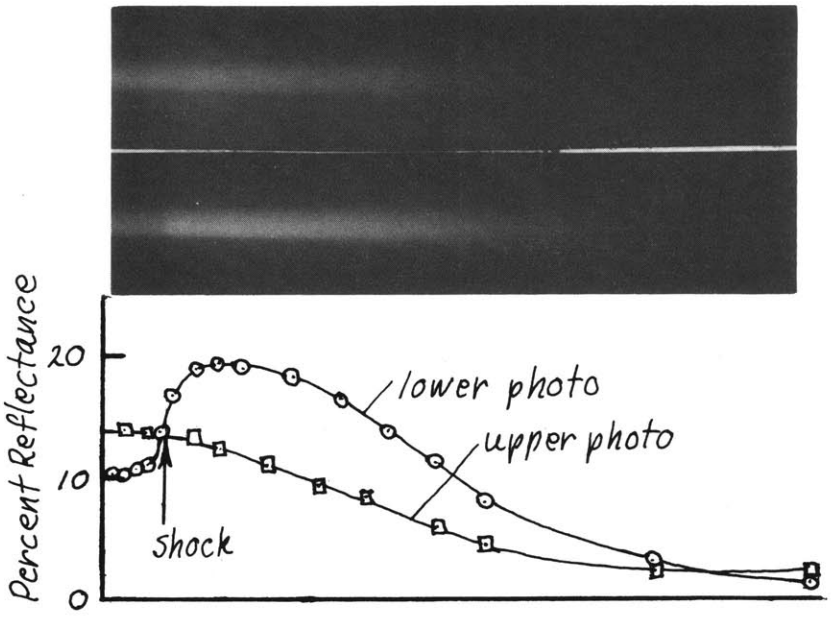

Figure 11: Photographs from the apparatus of Fig. 10 for a uniform aerosol (top), and with a shock (bottom). The plot, at bottom, of scattered light intensity, was obtained with a densitometer.

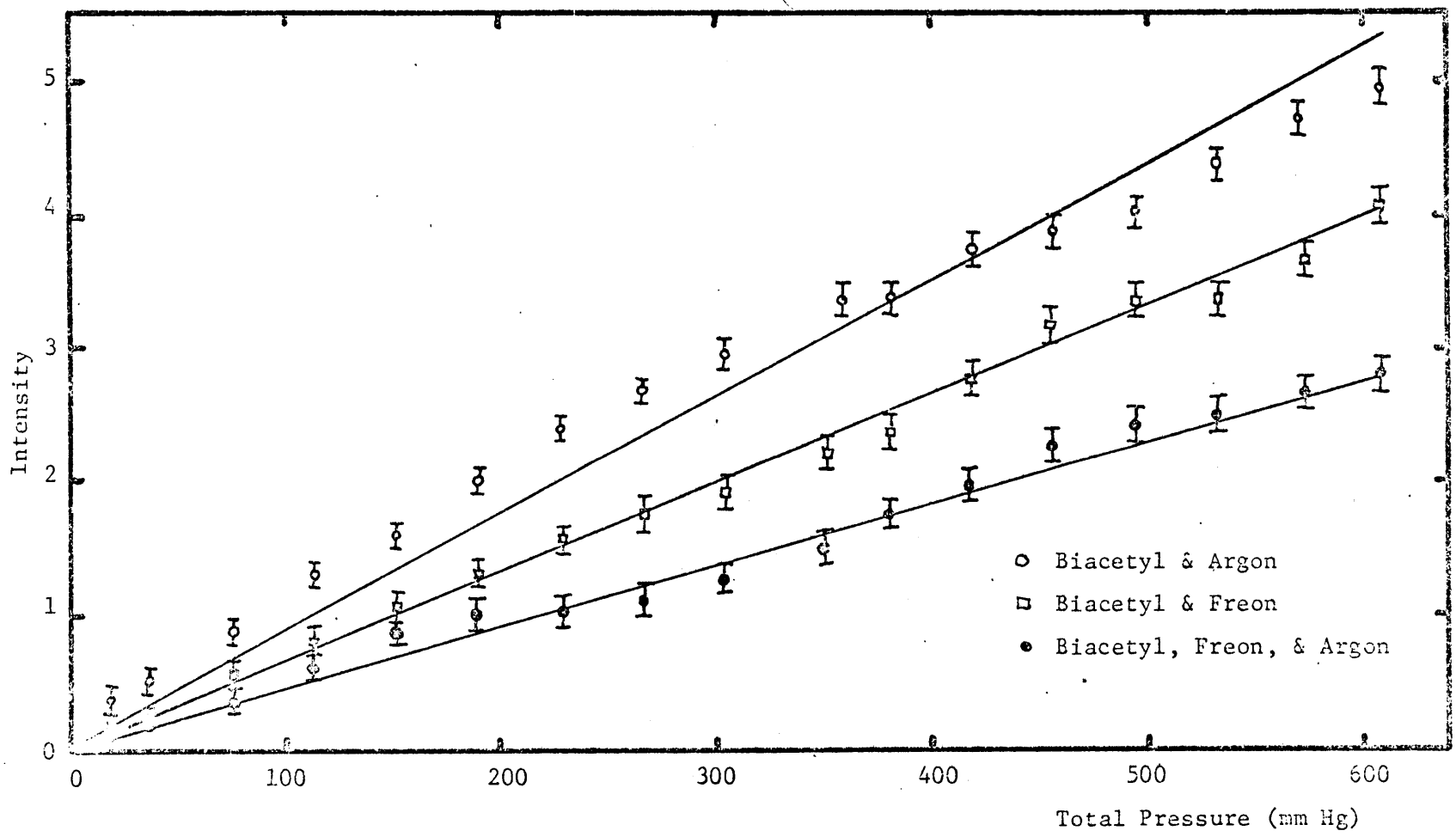

Figure 12: Phosphorescent intensity of mixtures of butanedione in argon-freon as a function of gas pressure.

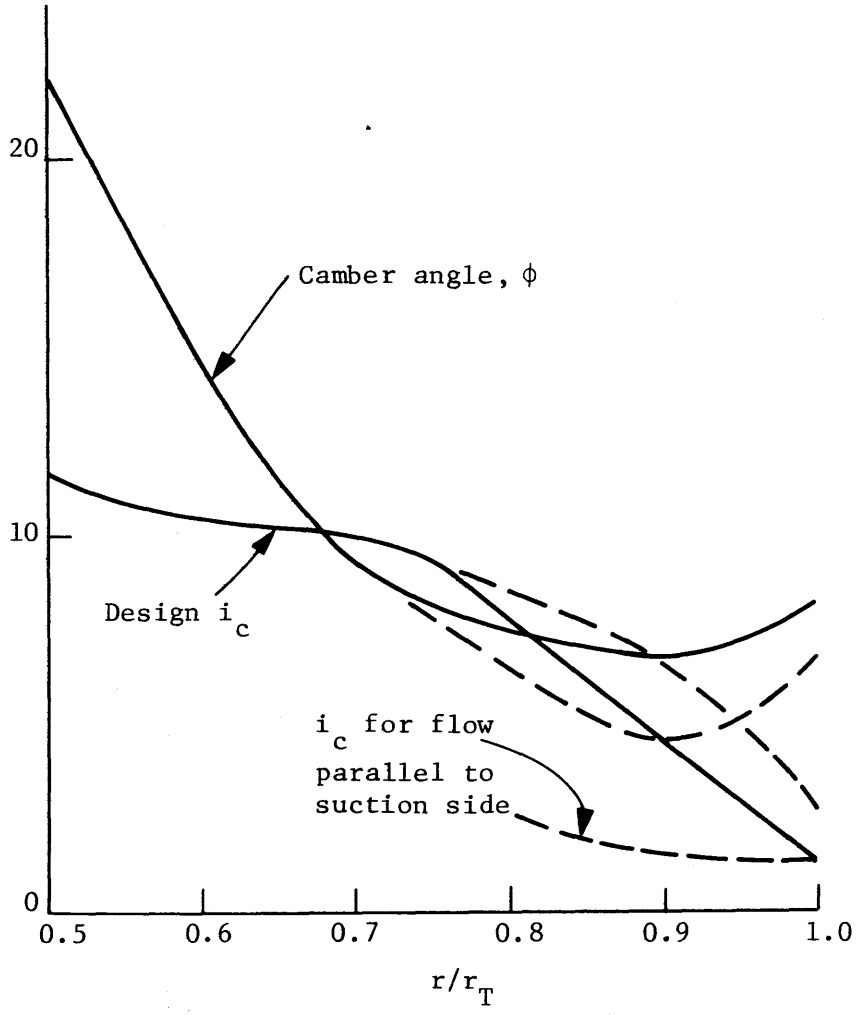

Figure 13

Design camber and incidence for the transonic rotor (full lines) compared to values given by Ref. (3) (dashed lines) and incidence parallel to suction side of blade.

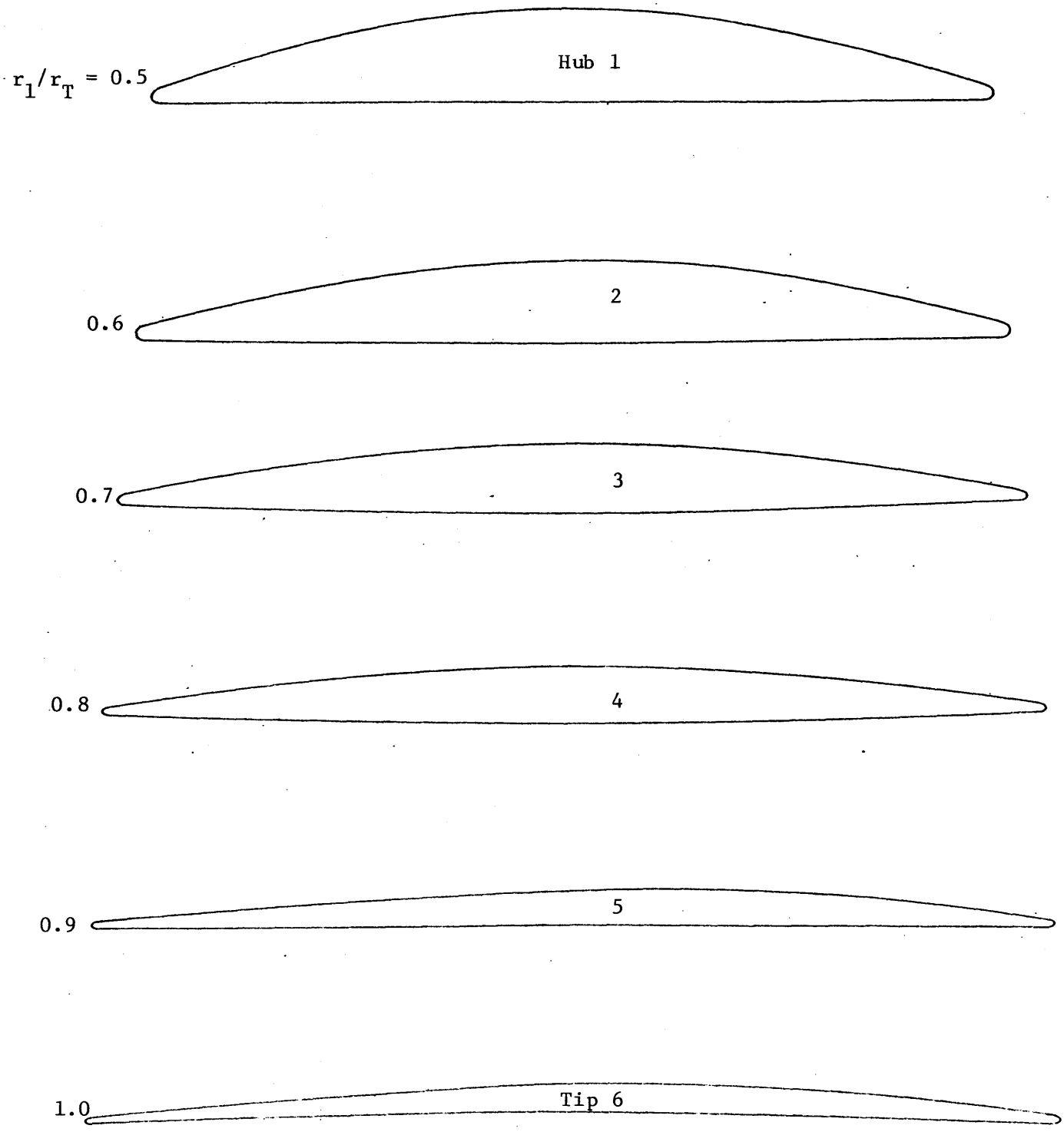

Figure 14: Blade cross sections projected onto conical streamsurfaces between r_1 and r_2 as given in Table III.

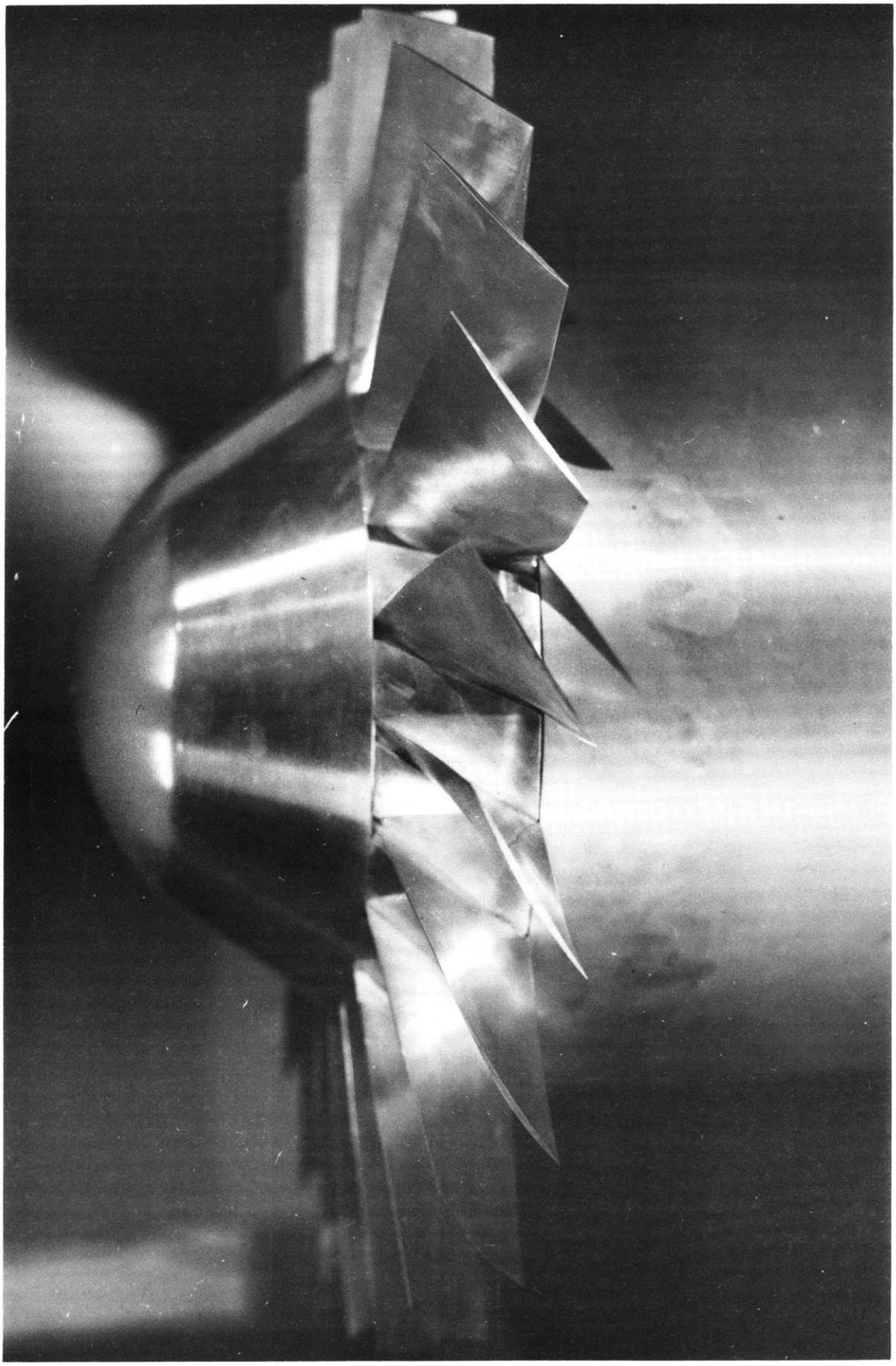

Figure 15: Transonic Compressor rotor with spinner and outlet hub fairing.

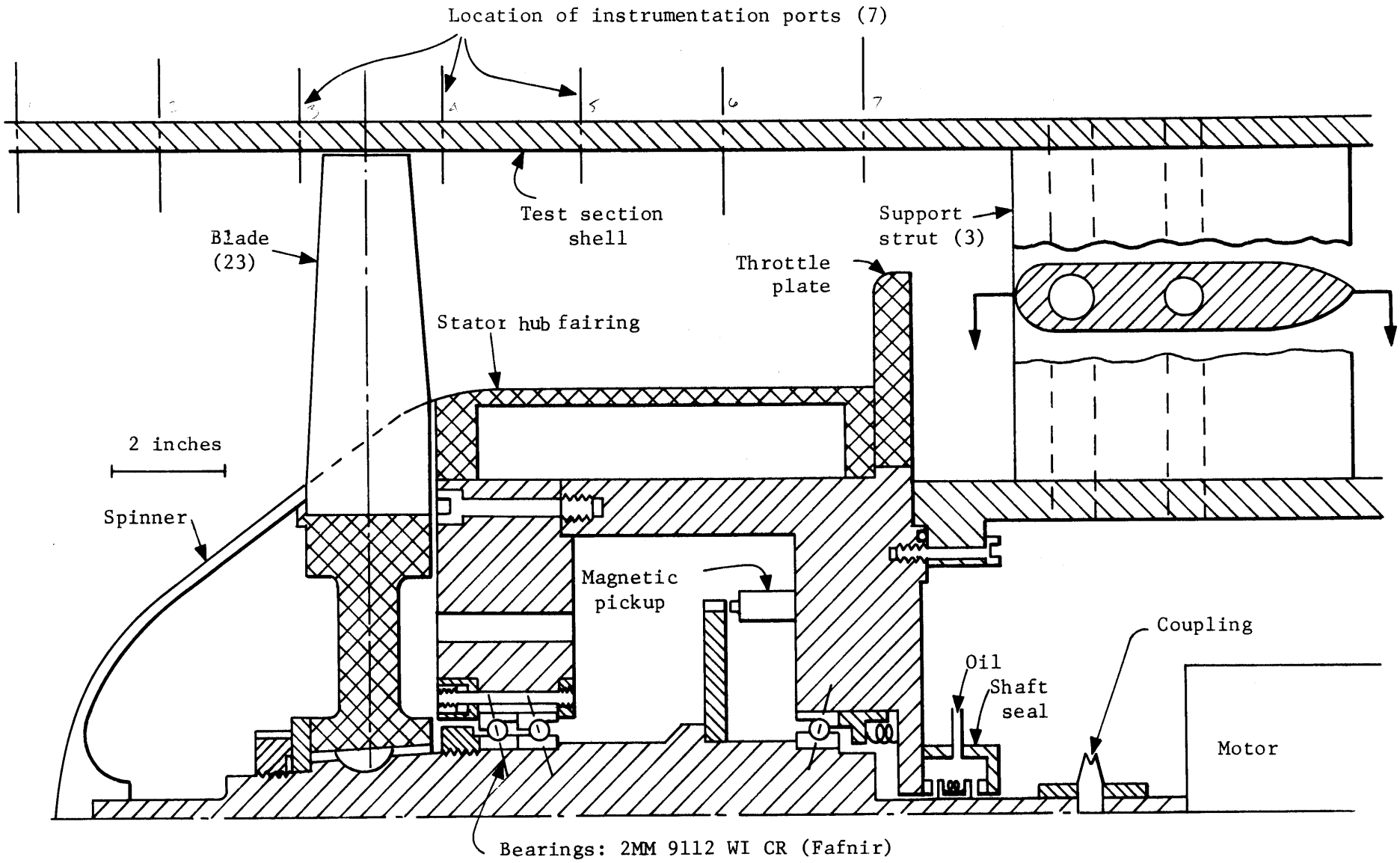

Figure 16: Scale drawing of the rotating assembly and test section, showing locations of rotor instrumentation ports, and throttle plate.

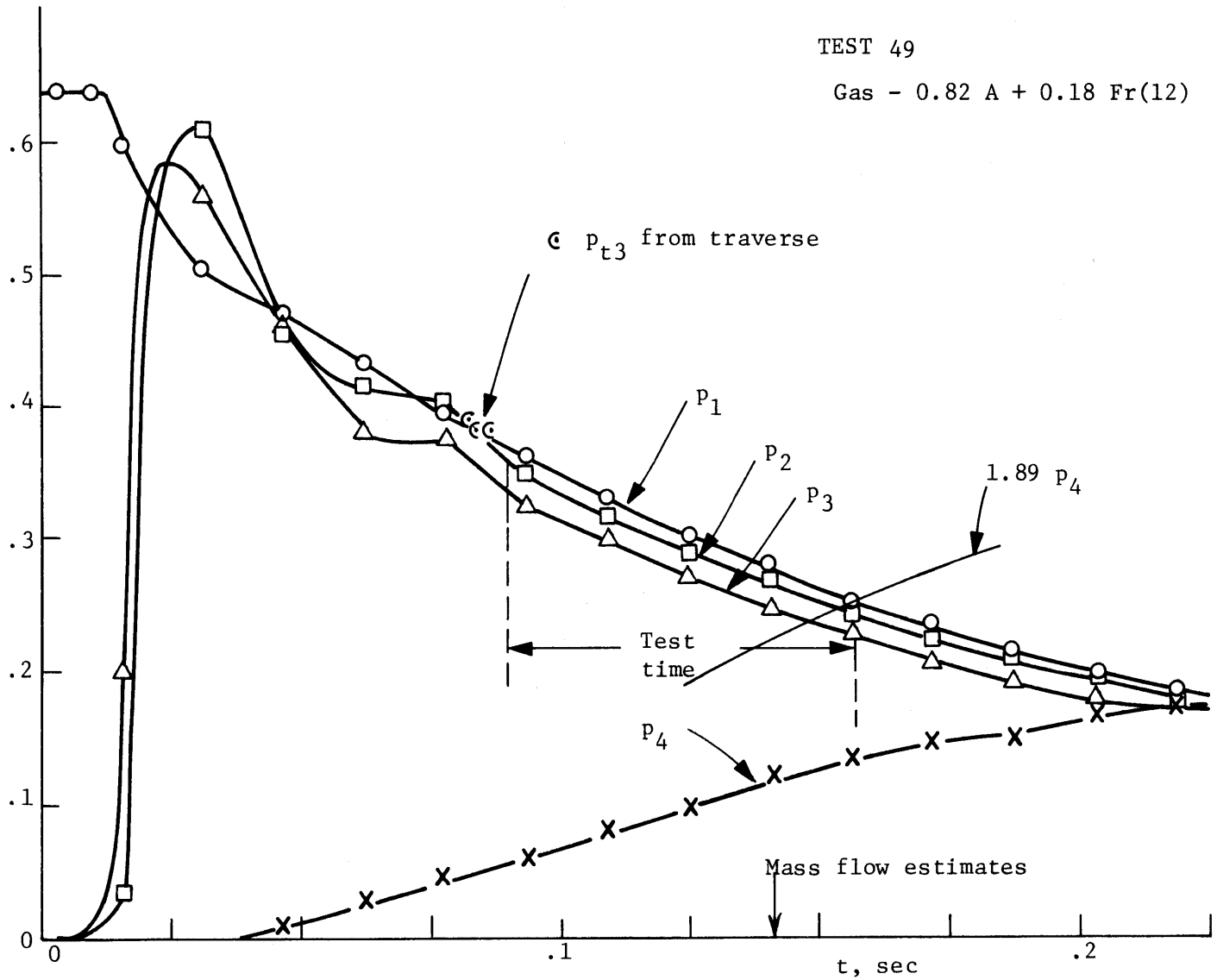

Figure 17: Variations of supply tank (p_1), compressor inlet (p_2), outlet (p_3) and dump tank (p_4) pressures with time during blowdown without rotor. Stagnation pressure in outlet annulus (p_{t3}) from traverse is also shown.

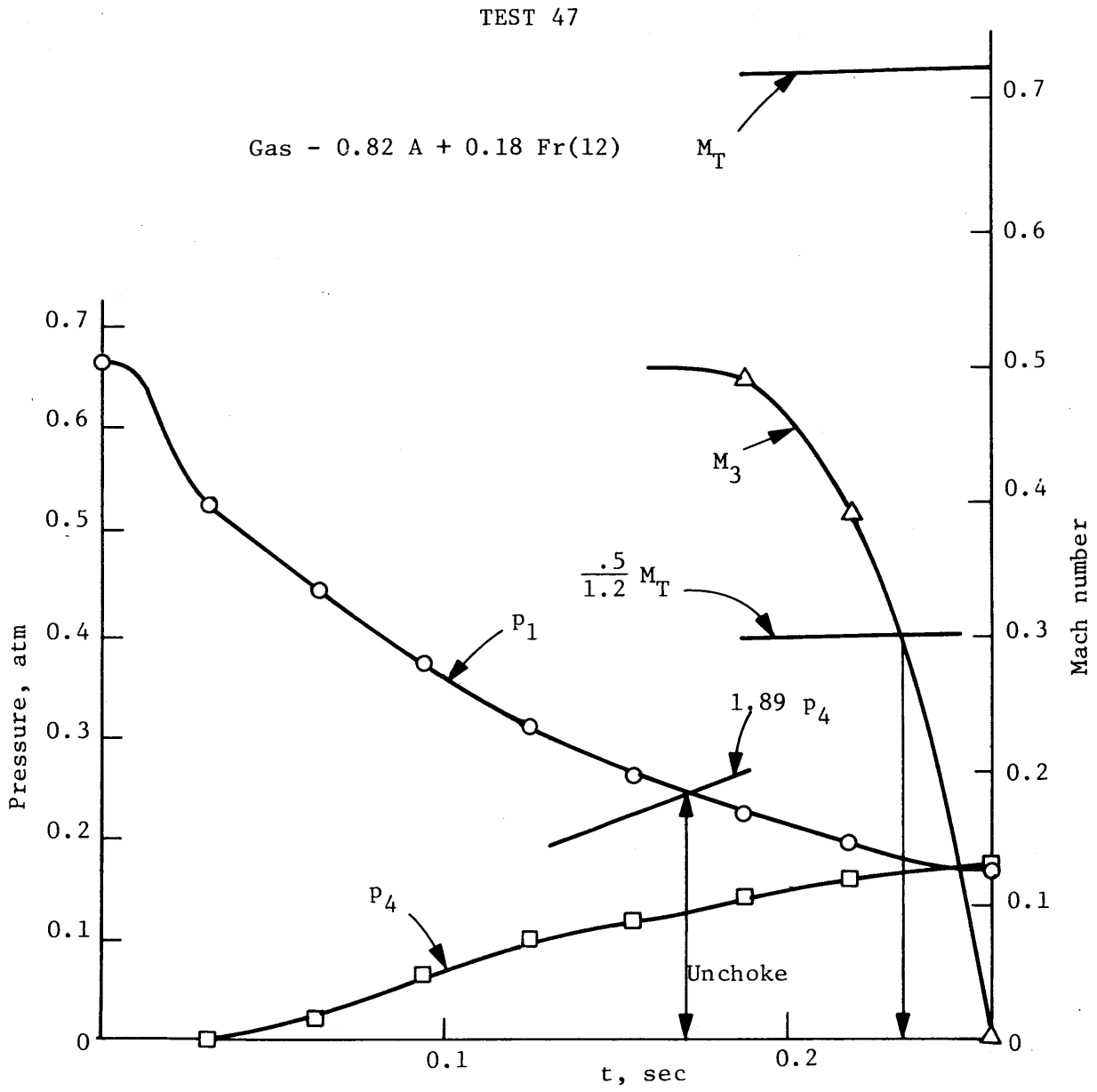

Figure 18: Variations with time of supply tank (p_1), and dump tank (p_4) pressures, tangential (M_T) and exit axial (M_3) Mach numbers for half-speed operation. A match point, where velocity triangles are near design, is reached after exit orifice unchokes.

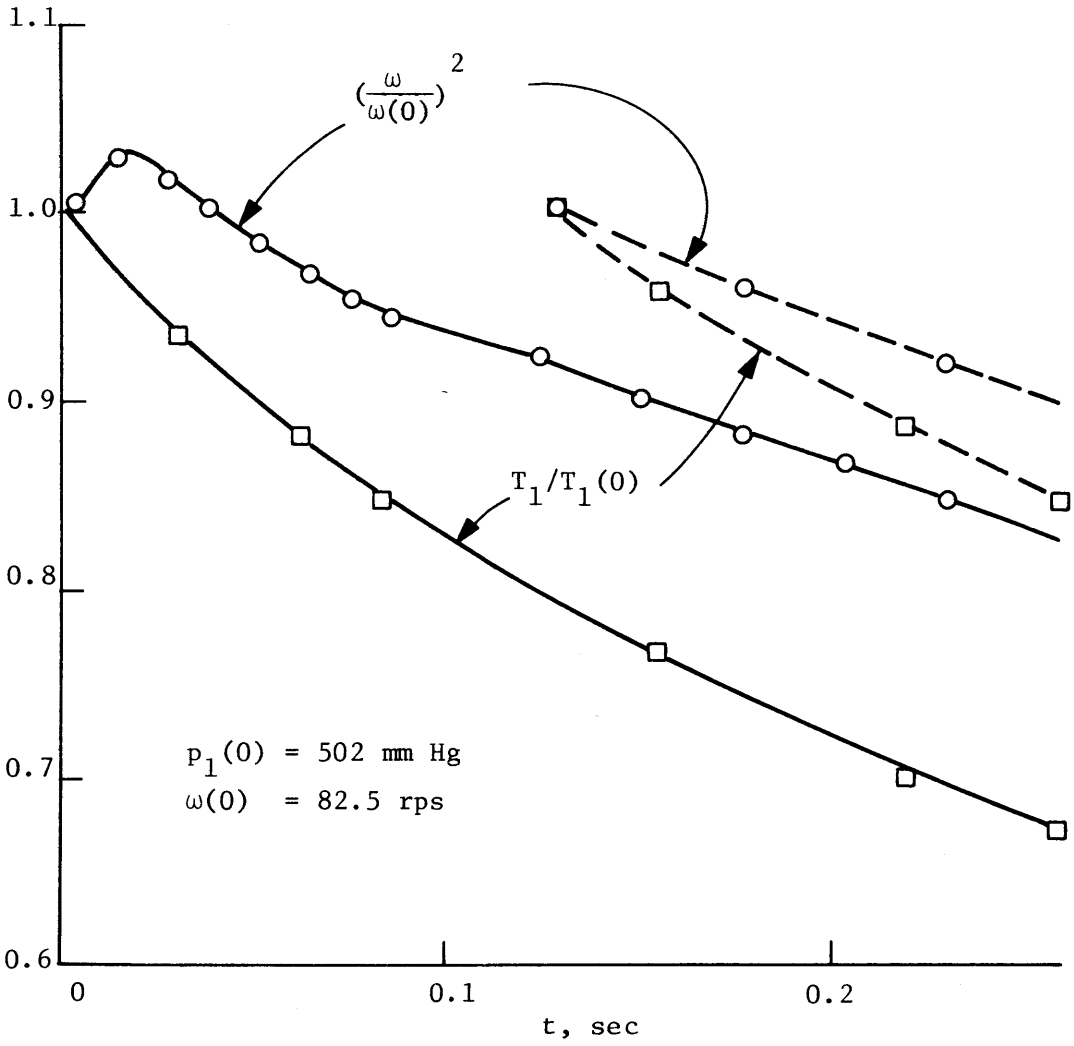

Figure 19: Variations of the square of rotor speed (ω^2) and stagnation temperature (T_1) with time, showing non-constant Mach number due to mismatch of exit orifice for half-speed operation.

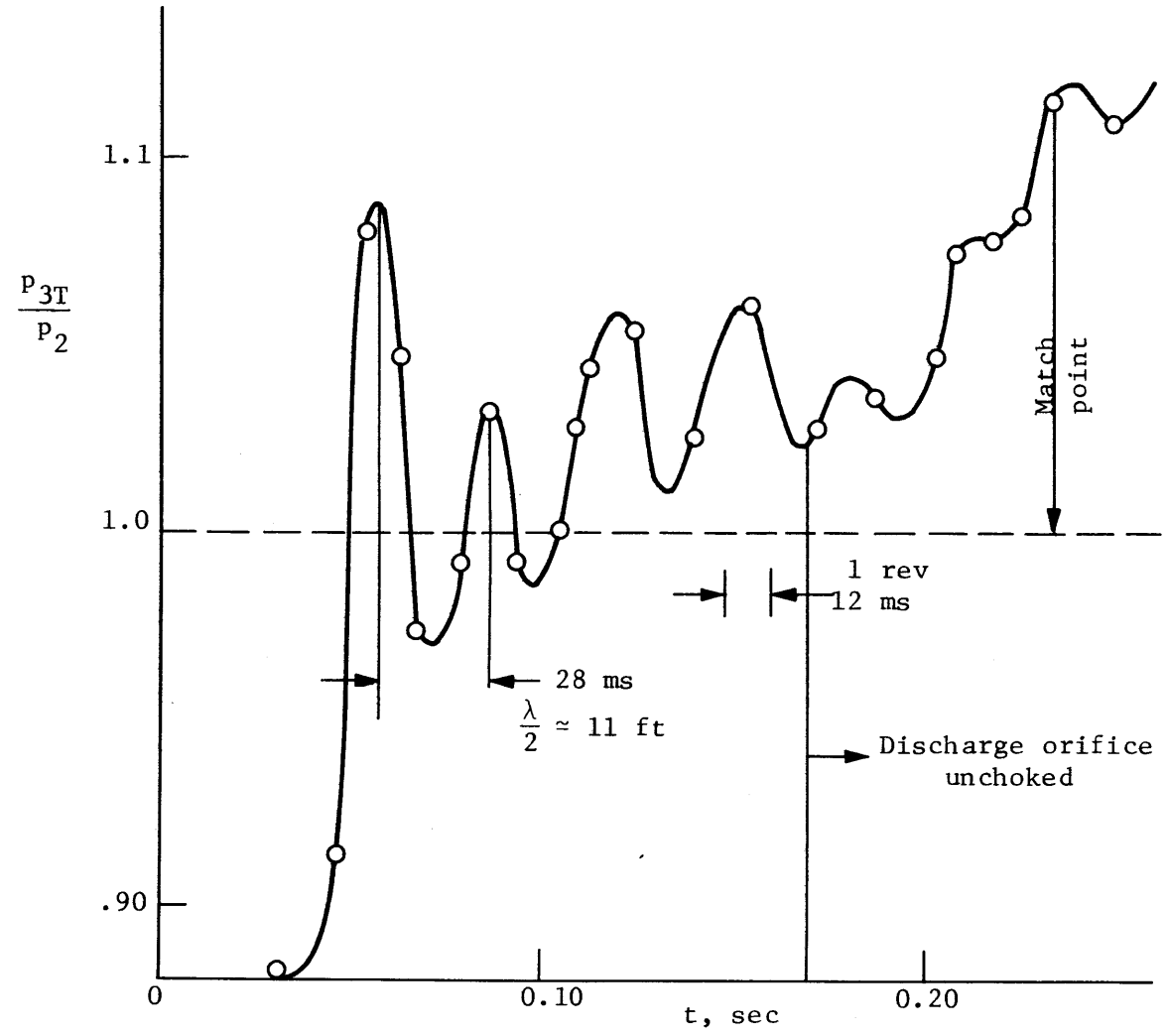

Figure 20: Static pressure ratio as function of time for half-speed operation, showing oscillations, apparently due to wave in supply tank, and match point near end of run.

TEST 47

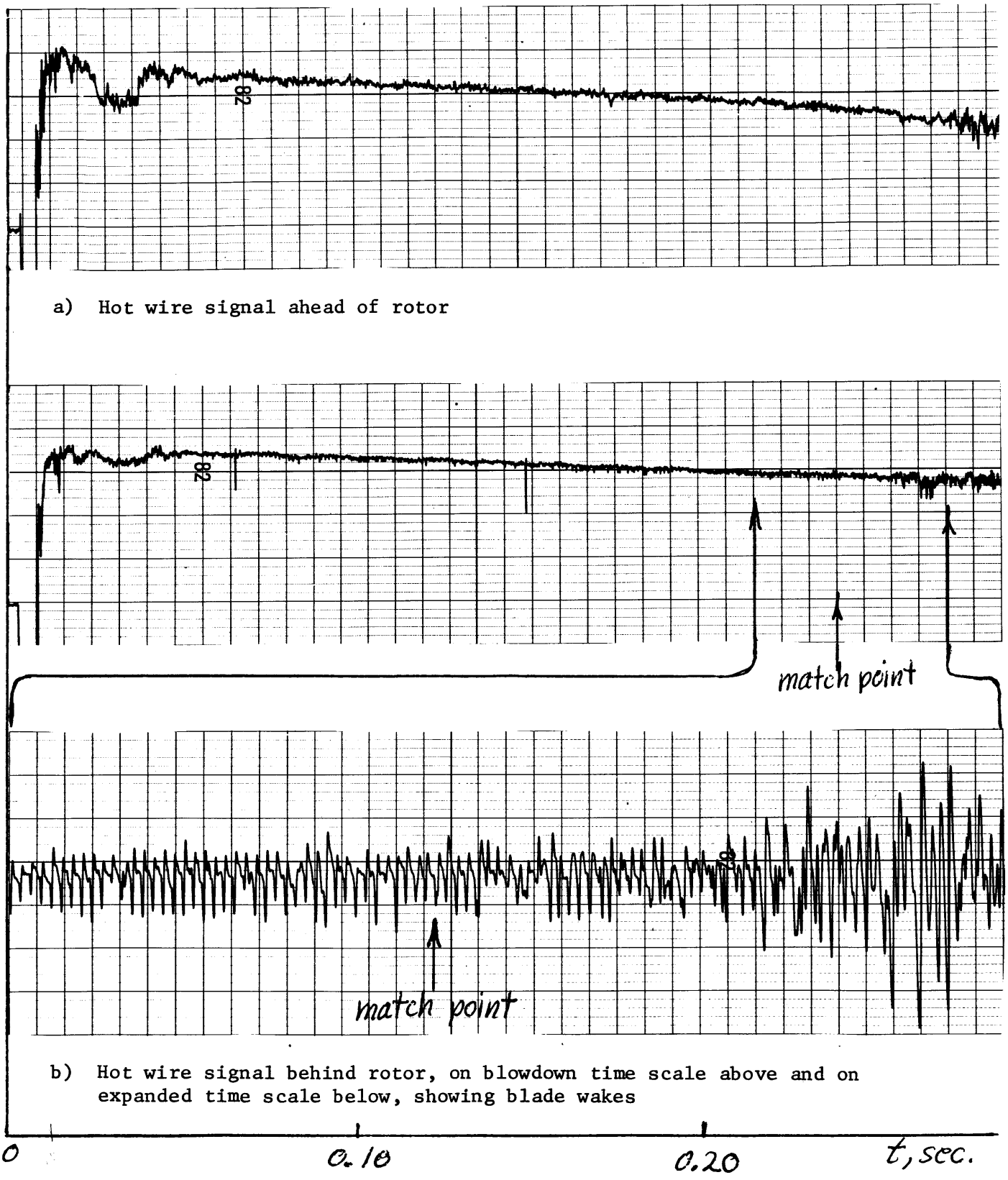

a) Hot wire signal ahead of rotor

b) Hot wire signal behind rotor, on blowdown time scale above and on expanded time scale below, showing blade wakes

Figure 21: Hot wire signals from constant temperature radial wires at mid-span in half-speed run.

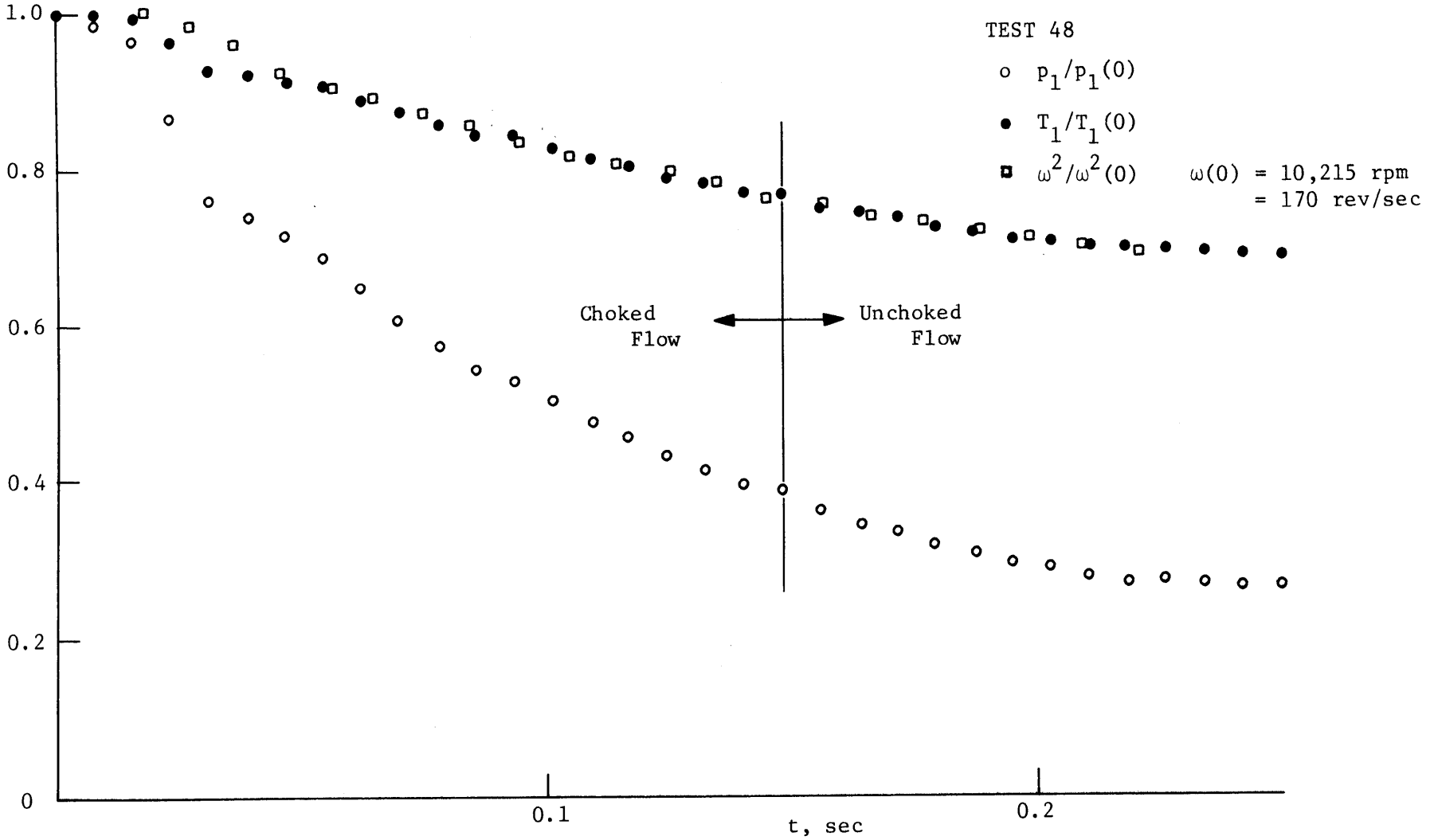

Figure 22: Variations of the square of rotor speed (ω^2) and stagnation temperature (T_1) (calculated from stagnation pressure) with time for full-speed near-design experiment, showing nearly exact constancy of tangential Mach number during test time.

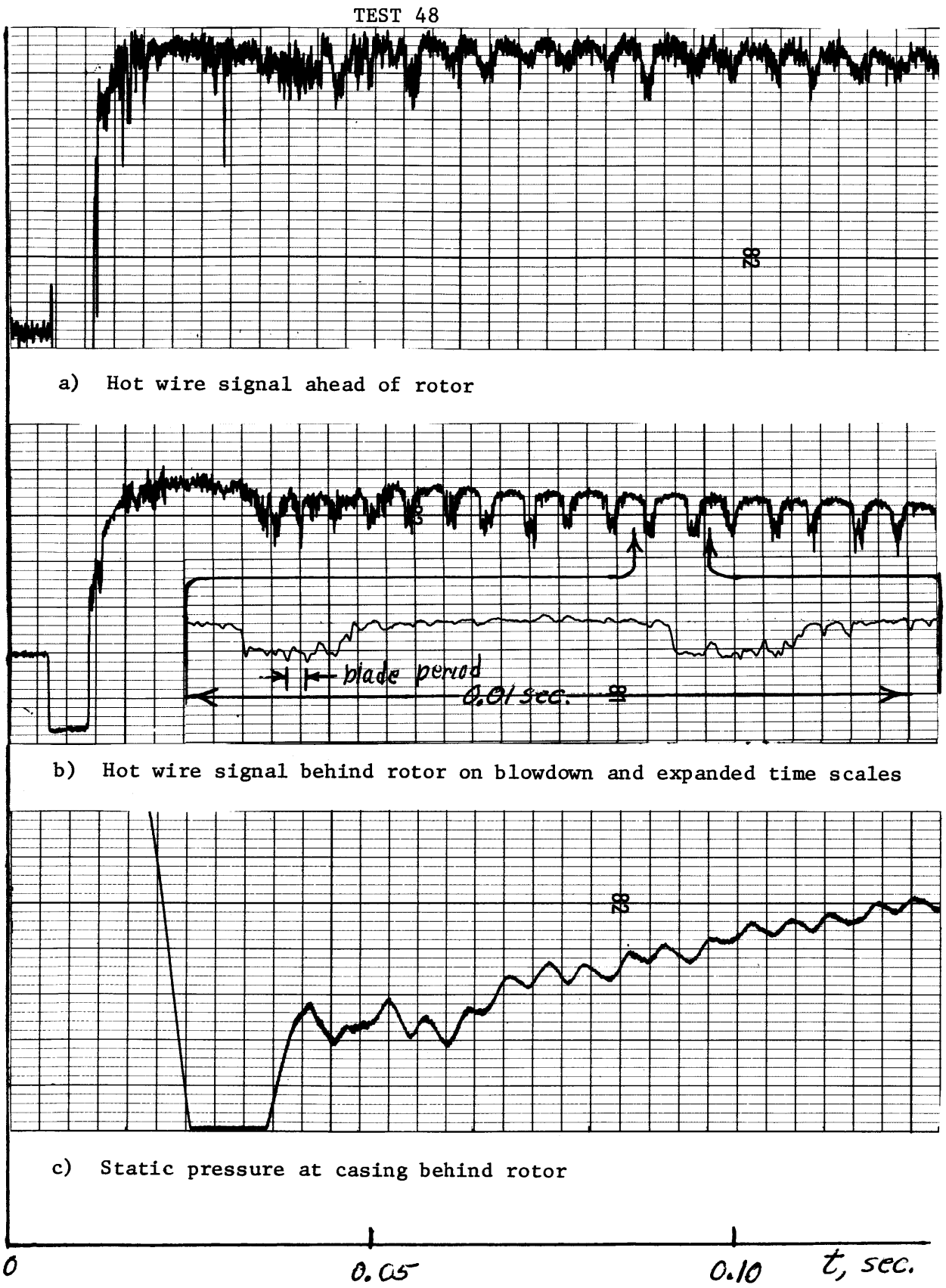

Figure 23: Hot wire signals from constant-temperature radial hot wires upstream and downstream of rotor for full-speed run with (two-cell) rotating stall, together with downstream static pressure.

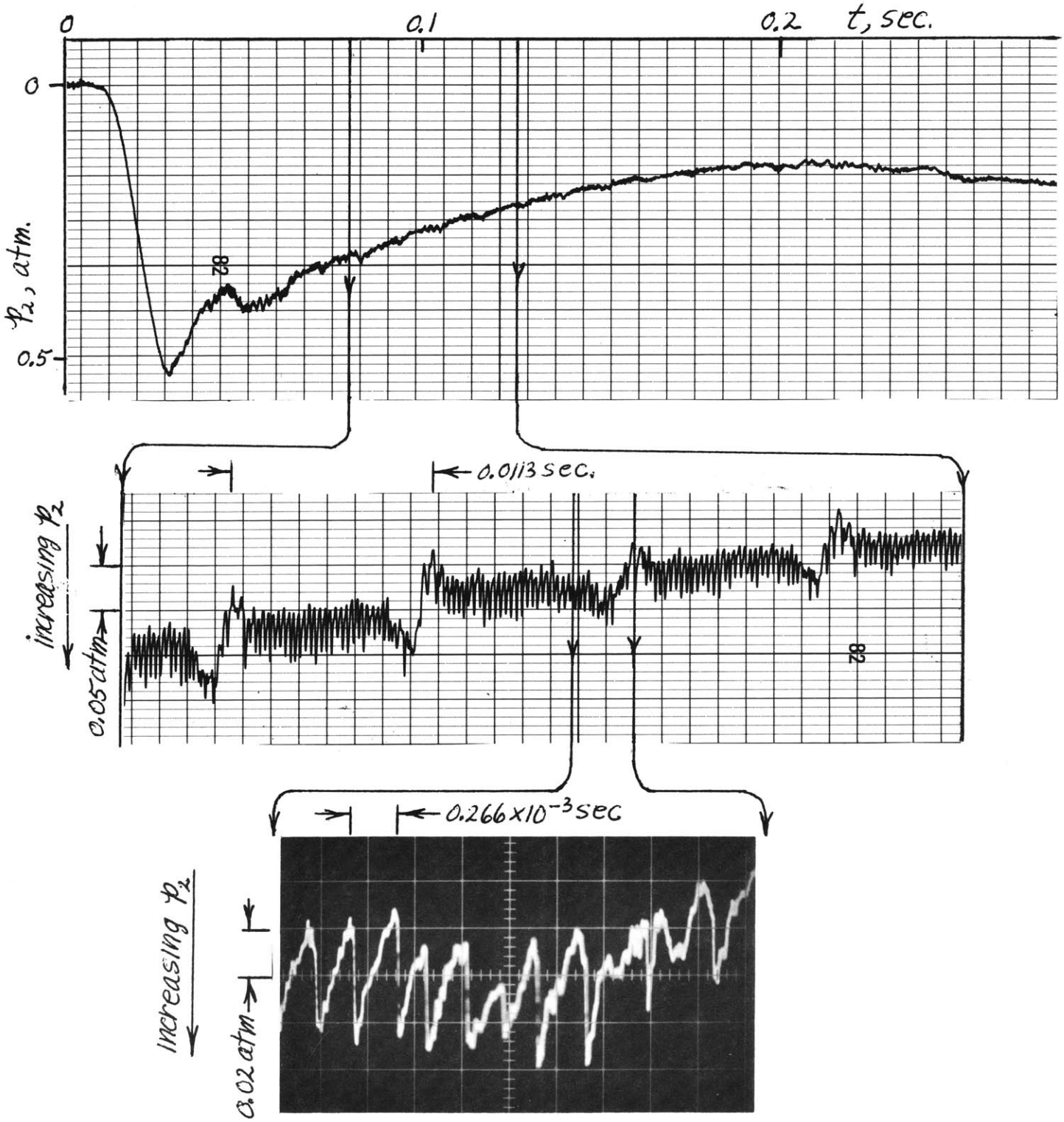

Figure 24: Static pressure upstream of rotor on three time scales, for run with (single cell) rotating stall. At top is blowdown time scale. In the center, several stall periods are displayed, and at the bottom, details of pressure for a few blade passing periods.

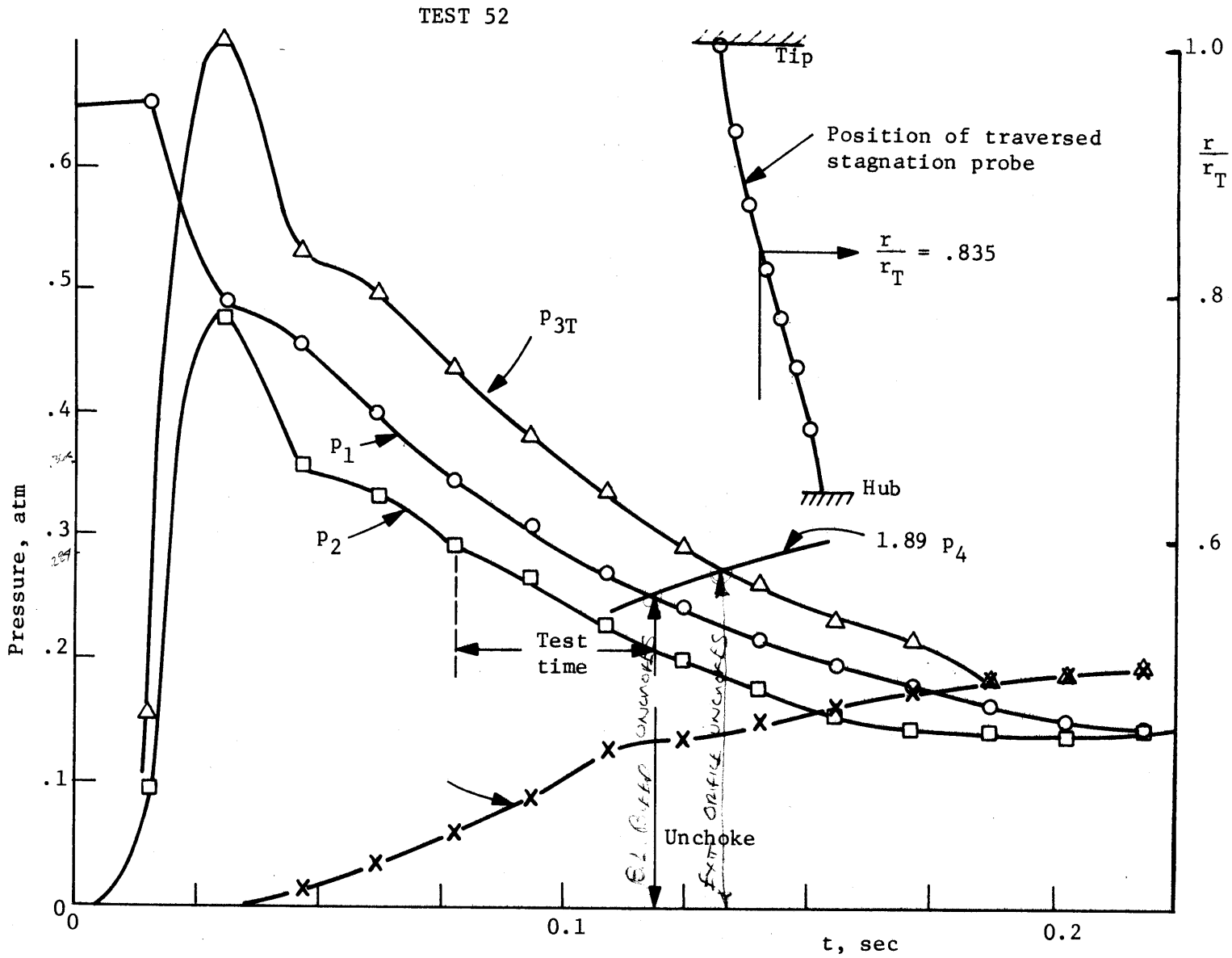

Figure 25: Variations of supply tank (p_1), rotor inlet (p_2), rotor outlet (p_{3T}) and dump tank pressures for a near-design full speed run without stall. The position of the downstream traversing stagnation probe as a function of time is shown at upper right.

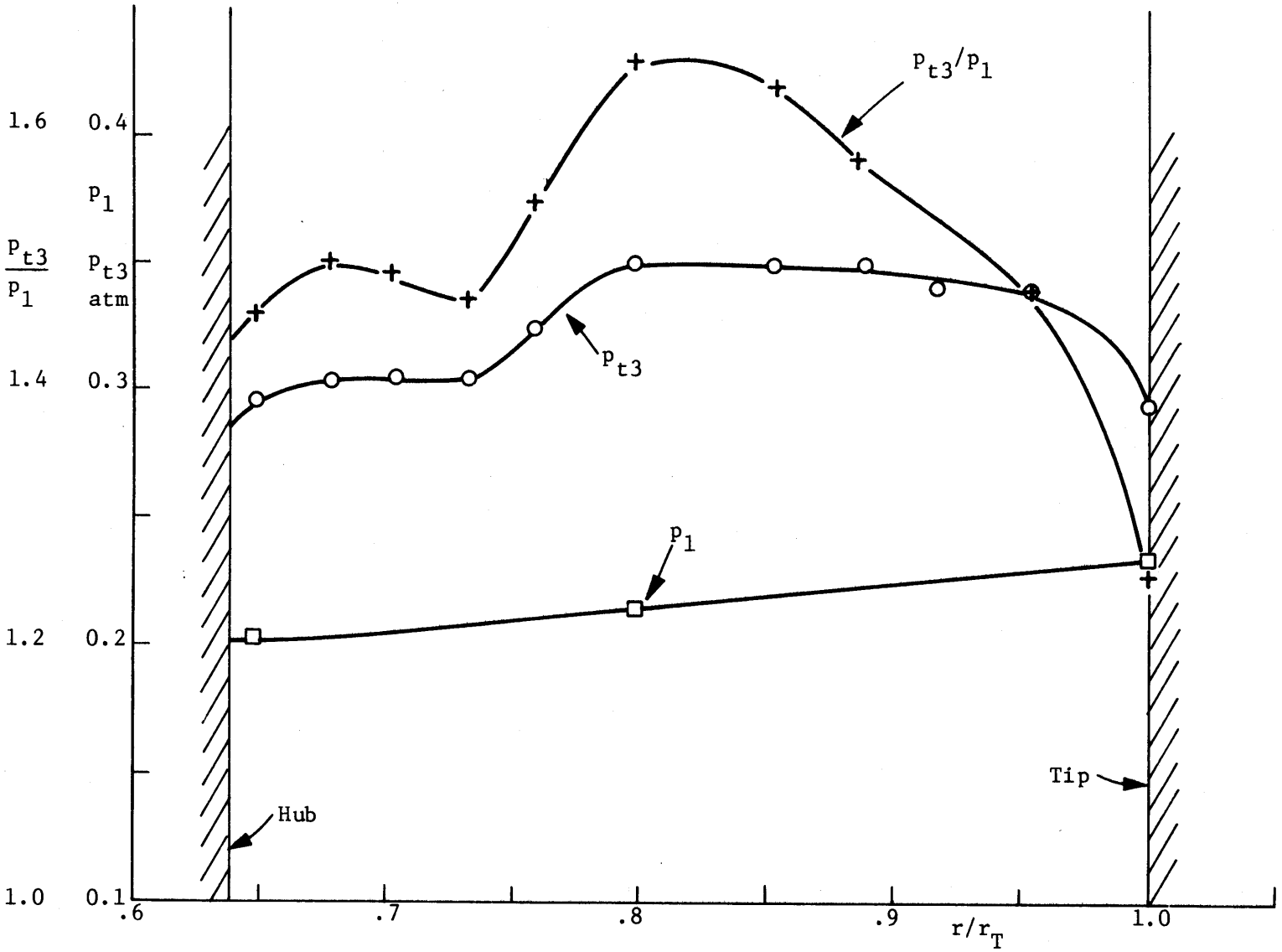

Figure 26: Downstream stagnation pressure, upstream stagnation pressure, and the resulting pressure ratio as functions of radius for the run of Fig. 25.

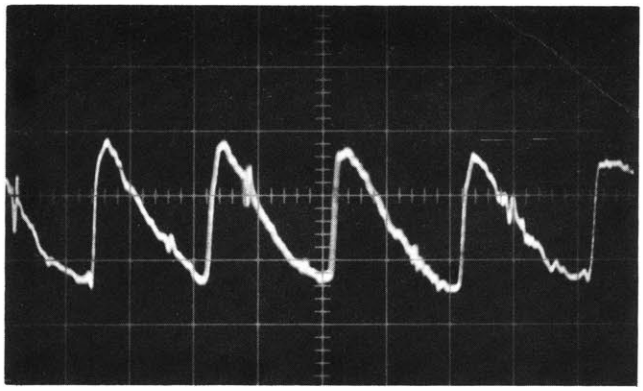

Figure 27: Upstream static pressure for the run of Fig. 25, showing the shocks and expansions for a few blade passing periods.

REFERENCES

1. Chapman, D. R., "Some Possibilities of Using Gas Mixtures other than Air in Aerodynamic Research," NACA Rep. 1259 (1956).

2. Schlichting, H., Boundary Layer Theory, McGraw Hill, 563 (1960).

3. Sinclair, D., and La Mer, V. K., "Light Scattering as a Measure of Particle Size in Aerosols," Chem. Rev., 44, 245-267 (1949).

4. Epstein, A. H., "Fluorescent Gaseous Tracers for Flow Visualization," S.M. Thesis, Dept. of Aeronautics and Astronautics, M.I.T. (1971).

5. "Aerodynamic Design of Axial-Flow Compressors,"NASA SP-36 (1965).